TALLINN UNIVERSITY OF TECHNOLOGY
SCHOOL OF ENGINEERING
Department of Materials and Environmental Technology

STUDY OF OPTOELECTRONIC PROPERTIES OF $Cu_2Zn(Sn,Sb)S_4$ MONOGRAIN POWDERS AND CORRESPONDING SOLAR CELLS

$Cu_2Zn(Sn,Sb)S_4$ MONOTERAPULBRITE JA NEIL PÕHINEVATE PÄIKESEPATAREIDE OPTOELEKTROONSETE OMADUSTE UURINGUD

MASTER THESIS

Üliõpilane: Seyyedmahan Khatami

Üliõpilaskood: 194314KAYM

Juhendaja: Professor Maarja Grossberg

Tallinn 2021

AUTHOR'S DECLARATION

Hereby I declare that I have written this thesis independently.
No academic degree has been applied for based on this material. All works, major viewpoints and data of the other authors used in this thesis have been referenced.

"....." ..... 20…..

Author: Seyyedmahan Khatami

Thesis is in accordance with terms and requirements

"....." ..... 20….

Supervisor: ….....
/signature/

Accepted for defence

"....."..... 20… .

Chairman of theses defence commission: .....
/name and signature/

Non-exclusive licence for reproduction and publication of a graduation thesis[1]

I _____ Seyyedmahan Khatami _____ (author's name)

1. grant Tallinn University of Technology free licence (non-exclusive licence) for my thesis
____ Study of optoelectronic properties of $Cu_2Zn(Sn,Sb)S_4$ monograin powders and corresponding solar cells ___,
(*title of the graduation thesis*)

supervised by _____Maarja Grossberg_____,
(*supervisor's name*)

1.1 to be reproduced for the purposes of preservation and electronic publication of the graduation thesis, incl. to be entered in the digital collection of the library of Tallinn University of Technology until expiry of the term of copyright;

1.2 to be published via the web of Tallinn University of Technology, incl. to be entered in the digital collection of the library of Tallinn University of Technology until expiry of the term of copyright.

2. I am aware that the author also retains the rights specified in clause 1 of the non-exclusive licence.

3. I confirm that granting the non-exclusive licence does not infringe other persons' intellectual property rights, the rights arising from the Personal Data Protection Act or rights arising from other legislation.

21.05.2021

[1] *The non-exclusive licence is not valid during the validity of access restriction indicated in the student's application for restriction on access to the graduation thesis that has been signed by the school's dean, except in case of the university's right to reproduce the thesis for preservation purposes only. If a graduation thesis is based on the joint creative activity of two or more persons and the co-author(s) has/have not granted, by the set deadline, the student defending his/her graduation thesis consent to reproduce and publish the graduation thesis in compliance with clauses 1.1 and 1.2 of the non-exclusive licence, the non-exclusive license shall not be valid for the period.*

Department of Materials and Environmental technology

THESIS TASK

Student: Seyyedmahan Khatami, 194314KAYM

Study programme: Materials and Processes for Sustainable Energetics

Main speciality: Materials for sustainable energetics

Supervisor: Prof. Maarja Grossberg, phone: 6203210

Thesis topic:

(in English) Study of optoelectronic properties of $Cu_2Zn(Sn,Sb)S_4$ monograin powders and corresponding solar cells

(in Estonian) $Cu_2Zn(Sn,Sb)S_4$ monoterapulbrite ja neil põhinevate päikesepatareide optoelektroonsete omaduste uuringud

Thesis main objectives:

1. To familiarize with photoluminescence and Raman spectroscopy methods
2. To learn the analysis process of photoluminescence spectra by studying the emission of Sb alloyed Cu_2ZnSnS_4 monograin powders
3. To gain knowledge about defects and radiative recombination mechanisms in Sb alloyed Cu_2ZnSnS_4 monograin powders

Thesis tasks and time schedule:

No	Task description	Deadline
1.	Photoluminescence and Raman measurements of Cu_2ZnSnS_4 monograin powders. Writing literature review.	February 2021
2.	Analysis of the obtained experimental data.	April 2021
3.	Writing of a master's thesis.	May 2021

Language: English **Deadline for submission of thesis:** 21 May 2021

Student: Seyyedmahan Khatami "....."……..201….a

Supervisor: Maarja Grossberg "....."…….201….a

/signature/

Head of study programme: Sergei Bereznev "....."…….201.a

/signature/

CONTENTS

PREFACE

The topic of this master's thesis was initiated and the thesis work supervised by Prof. Maarja Grossberg, the Head of the Laboratory of Optoelectronic Materials Physics in the Department of Materials and Environmental Technology. Major part of the thesis work was carried out in the Laboratory of Optoelectronic Materials Physics. The studied monograin powders were synthesized by Dr. Kristi Timmo in the Laboratory of Photovoltaic Materials Research. Monograin layer solar cells were prepared by Dr. Maris Pilvet in the Laboratory of Photovoltaic Materials Research. PhD student Reelika Kaupmees and Dr. Mati Danilson assisted author in photoluminescence and I-V(T) as well as EQE data collecting, respectively. Dr. Arvo Mere performed the XRD analysis and Dr. Valdek Mikli made the EDX analysis of the studied samples.

I cannot express enough appreciation to my supervisor, professor Maarja Grossberg for her continued support and encouragement. I offer my sincere appreciation for the learning opportunities provided by associate professor Sergei Bereznev and Tallinn University of Technology. My completion of this project could not have been accomplished without the support of the members of the Laboratory of Photovoltaic Materials Research and Laboratory of Optoelectronic Materials Physics, and special thanks to Reelika Kaupmees, who helped me a lot.

The study was financially supported by the Estonian Research Council grant PRG1023 "Sustainable, cost-efficient, flexible, lightweight and semitransparent multinary chalcogenide based solar cells for building integrated photovoltaics" and by the European Regional Development Fund project TK141 "Advanced materials and high-technology devices for sustainable energetics, sensorics and nanoelectronics". In additon, the project "Center of nanomaterials technologies and research (NAMUR+)" (2014-2020.4.01.16-0123) is acknowledged.

Keywords: Photoluminescence spectroscopy, defects, Cu_2ZnSnS_4, Raman spectroscopy, Master's thesis.

List of abbreviations and symbols

ADS	Asymmetric double sigmoid function
BB	Band-to-band
BI	Band-to-impurity
BT	Band-to-tail
CdTe	Cadmium telluride
CIGS	Copper indium gallium diselenide
CZTS	Copper zinc tin sulfide
CZTSbS	Copper zinc tin antimony sulfide
CZTSe	Copper zinc tin selenide
E_g	Bandgap energy
E_{max}	PL band position
E_u	Urbach energy
EDX	Energy dispersive X-ray spectroscopy
EQE	External quantum efficiency
E_T	Thermal activation energy
Φ	Integrated luminescence intensity
γ_E	Average depth of the spatial electrostatic potential fluctuations
γ_B	Average depth of the band gap fluctuations
FF	Fill factor
FWHM	Full width at half maximum
I-V	Current-Voltage
I_{sc}	Short-circuit current
J_{sc}	Short-circuit current density
MGL	Monograin layer
PCE	Power conversion efficiency
PL	Photoluminescence
PMT	Photomultiplier tube
PV	Photovoltaic
SC	Solar cell
SEM	Scanning electron microscope
V_{OC}	Open-circuit voltage
XRD	X-ray diffraction

List of figures and tables

INTRODUCTION

Clean power is an essential part of the future. Renewable energies have been growing during the 21st century. Technology and cost improvement are two practical factors that pave the way towards the widespread use of renewable energy technologies. Various forms of policies and regulatory support help expand these forms of energy instead of non-renewables. Recently, the European Commission has launched an ambitious European Green Deal program targeting climate-neutral Europe by 2050 [1], [2]. Renewable energy technologies play a key role in achieving the goals of the program. Renewables are cheaper, healthier, and help to stop climate change by decreasing greenhouse gas emissions. Besides, shreds of evidence show that cleaner power can stimulate the economy and prompt clean technology investment. Renewable power can be supported in various ways to grow as a new industry and achieve its potential to deliver a sustainable future. Flexibility is a fundamental characteristic of electricity systems today, and enhanced flexibility will enable the cost-effective incorporation of renewable generation into grids.

Electricity systems are already highly flexible, balancing fast-changing demand with supply. Power systems can improve their flexibility through operational and technical measures matched to the grid's renewables' characteristics. Lower-cost operational measures include more accurate forecasting, coordinating with neighboring connected grids, and flexible demand response programs. Additionally, higher-cost measures like electricity storage are rapidly reducing costs, and increasingly smart and automated grids are emerging. Together, these factors should make higher shares of renewables technically feasible and economical.

The application of solar cells has been considered due to the extensive consumption of fossil fuels in the mid-1970s. In the last few years, the rate of installed solar power capacity has clearly outpaced net installations of other renewables (see Figure 0-1) as well as both fossil fuel and nuclear power capacity. Till now, there are three generations of solar cells: crystalline Si technologies, thin film solar cells, and emerging technologies, all of them having their advantages and disadvantages. The most mature of these are crystalline Si technologies that currently dominate the photovoltaics (PV) market, but in addition to having the largest ecological footprint of the commercialized PV technologies, their applications are limited due to the rigid structure of the PV modules. The main aim of second-generation thin film solar cells represented by $Cu(In,Ga)Se_2$ and CdTe was to reduce the cost of design by implementing very thin layers of absorber material enabled by their excellent absorption coefficients. However, the Cd and Te's toxicity and the limited resources of expensive In and Ga have hindered the large-scale

use of these technologies. As a result, several emerging PV technologies enabling further cost-reduction and versatile applications are being developed, the mixed-halide perovskites, kesterites, and antimony dichalcogenide technologies frontrunners there. In addition, hybrid and tandem PV technologies are being developed as emerging PV concepts.

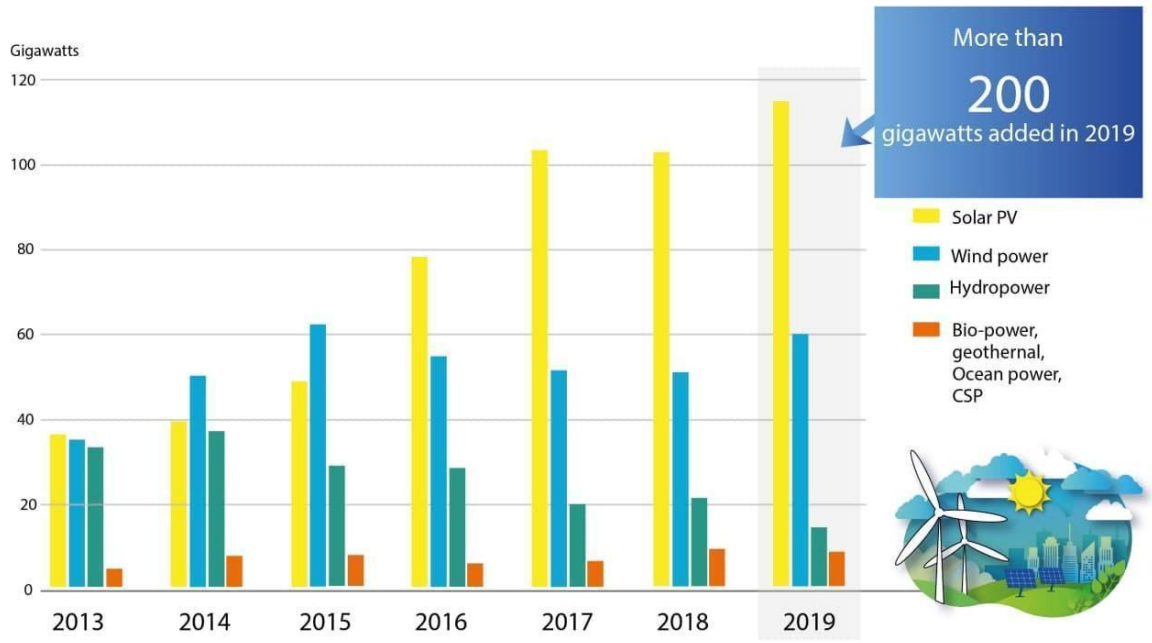

Figure 0-1. Annual global additions of renewable power capacity in 2013-2019 [3].

Among the emerging PV technologies, the kesterites $Cu_2ZnSn(S,Se)_4$ (CZTSSe) have the major advantage of being fully environmentally friendly as consisting of earth-abundant and non-toxic elements. CZTSSe based solar cells have already demonstrated considerable power conversion efficiencies (PCE, 12.6%) and stability, being in the leading position in emerging sustainable PV technologies; however, significant improvement in PCE is still needed for commercialization [4]. To bring the CZTSSe PCE to the next level, one needs to solve the currently shown key issue that is strong recombination of photogenerated charge carriers via various routes leading to short minority carrier lifetime (that is a magnitude lower than in CIGSe, CdTe, etc.) and diffusion length and resulting in large open-circuit voltage deficit of CZTSSe SCs[5]–[8].One of the promising approaches is implementing cation alloying of the CZTSSe absorber to homogenize the materials phase and defect composition, including reducing deep recombination centers and band tailing aiming at reduced bulk recombination. This Master thesis is dedicated to the study of the influence of antimony (Sb) alloying of the kesterite Cu_2ZnSnS_4 monograins on the defect structure of this material. There is very little information about the influence of Sb on the properties and performance of the

kesterite solar cells, and it is the first time when Sb is introduced to the kesterite monograins. The defect structure and related recombination mechanisms of the $Cu_2Zn(Sn,Sb)S_4$ monograins are studied by temperature-dependent photoluminescence spectroscopy and complemented by the external quantum efficiency (EQE) and current-voltage (I-V) characterization of the corresponding monograin layer solar cells.

1. Literature review

During past decades, solar technology has been drastically improved. The energy which is prepared by the sun for an hour meets the global energy demand for a year. While it has been widely criticized for being expensive or inefficient, solar energy has now proved to be extremely beneficial not only for the environment but also for the private economy. The flexibility of usage, low cost of maintenance, and being eco-friendly makes solar technology favorable. Despite numerous positive consequences of using solar cells, the power conversion efficiencies of photovoltaics and their cost-effectiveness are still limited, restraining the widespread use of solar electricity.

In addition to the system-related issues, the widespread use of photovoltaics depends on the cost-effectiveness and sustainability of the constituent materials, the absorber material is the key element. In addition to optimal band gap energy, high absorption coefficient, and favorable current transport properties, the absorber material should be sustainable. One of the most promising emerging photovoltaic absorbers is the so-called kesterite $Cu_2ZnSn(S,Se)_4$ (CZTSSe) that consists of earth-abundant elements (see Figure 1-1) and has suitable semiconducting properties for solar energy conversion. The first kesterite solar cell was fabricated in 1997, showing PCE of 0.66% [9]. To date, with kesterite CZTSSe, a record power conversion efficiency of 12.6% has been achieved, and further improvements are required to reach the high efficiencies needed for the industrial implementation [4]–[10]. To bring the CZTSSe PCE to the next level, one needs to solve the currently shown key issue that is strong recombination of photogenerated charge carriers via various routes leading to short minority carrier lifetime (that is a magnitude lower than in CIGSe, CdTe, etc.) and diffusion length and resulting in large open-circuit voltage deficit of CZTSSe solar cells [5]–[8]. One of the promising approaches is implementing cation alloying of the CZTSSe absorber to homogenize the materials phase and defect composition, including reducing deep recombination centers and band tailing aiming at reduced bulk recombination.

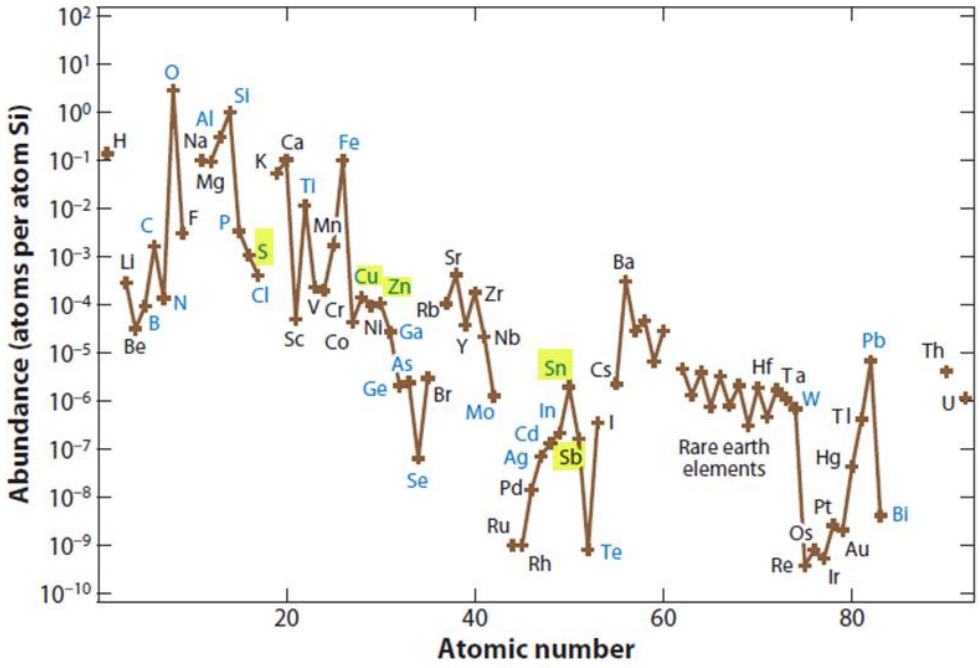

Figure 1-1. The abundance of elements in the Earth's crust and the sea [11].

However, several alloy configurations of CZTSSe have been studied, not yet resulting in higher power conversion efficiencies of the kesterite solar cells compared to the current record device [8]–[10], [12]. Some of the alloys have not been extensively studied, and their potential is not revealed yet, the substitution of tin (Sn) by antimony (Sb) among these. It is known that Sn-related deep defects such as Zn_{Sn}, Sn_{Zn}, $V_{Sn,}$ and Cu_{Sn} introduce harmful strong recombination centers to CZTSSe [6], [13]–[17]. Therefore, partial substitution of Sn with other elements is considered favorable for reducing the overall recombination losses in CZTSSe solar cell devices. This Master thesis is dedicated to the study of the influence of Sb alloying of the kesterite Cu_2ZnSnS_4 (CZTS) monograins on the defect structure of this material and to the performance of the corresponding monograin layer (MGL) solar cell devices.

1.1 Properties of kesterite Cu_2ZnSnS_4

Cu_2ZnSnS_4 is a p-type compound semiconductor that crystallizes in the tetragonal crystal structure. Kesterite structure with space group $I\bar{4}$ is proven to be the most stable ground state crystal structure of CZTS; however, it can also crystallize in stannite structure with space group $I\bar{4}2m$ [18], [19]. The difference between the two crystal

structures lies in the different atomic arrangements of isoelectronic Cu and Zn atoms in the crystal planes (see Figure 1-2). Due to the similarity of the cation size and the low energy difference between the stannite- and kesterite-related crystal structures, Cu-Zn cation disorder is present in CZTS [20]. It was found that the Cu-Zn disorder in CZTS follows a second-order phase transition with a critical temperature of T ≈ 533 K (260°C). In the studies of CZTS thin films and monograins annealed at different temperatures, a remarkable effect of the degree of Cu-Zn disordering on the band gap energy and the vibrational and optical spectra of CZTS has been observed [17],[21]–[24]. The presence of Cu-Zn disordering was found to introduce band gap energy fluctuations to the material, and an increase in the degree of disordering can lead to change in the band gap of CZTS up to 0.2 eV varying from around 1.4 to 1.6 eV (T = 300 K) in different studies. The presence of the band gap fluctuations has a severe effect on the corresponding solar cells' performance. The absorption coefficient of CZTS at 1.6 eV is about 10^4 cm^{-1} [21].

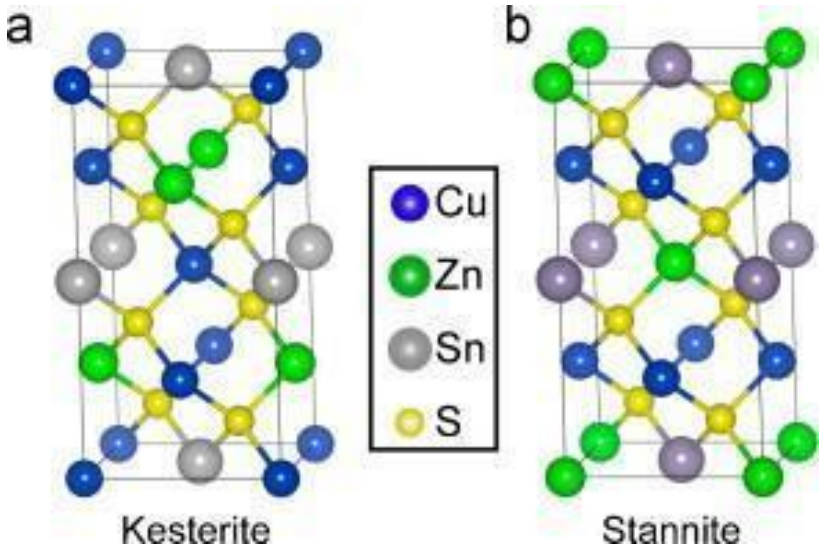

Figure 1-2. Kesterite and stannite crystal structures of CZTS [25].

Due to the Cu-Zn disorder in CZTS, this material contains high concentration of Cu_{Zn} and Zn_{Cu} antisite defects as Cu and Zn easily switch places in the crystal lattice. These two defects can also form a defect complex due to the very low formation energy.
According to first-principles calculations, the antisite defect Cu_{Zn} has the lowest and negative formation energy, meaning that this defect forms simultaneously and contributes the most to the p-type conductivity in kesterite CZTS [15]–[19]. However, till now, the highest solar cell efficiencies have been achieved with Cu-poor, Zn-rich, and Sn-stoichiometric CZTS absorbers in which the formation of Cu_{Zn} acceptor defect should be suppressed and the formation of shallow acceptor V_{Cu} promoted. The

corresponding defects' ionization energies are ~120 meV [26] and ~20 meV [27], respectively. It has been found that the Zn-rich and Cu-poor compositions of CZTS should also help to avoid the formation of detrimental Sn-related deep defects such as Cu_{Sn}, Sn_{Cu}, and Sn_{Zn}, which have ionization energies above 200 meV [15]. In addition to the isolated electronic defects, defect complexes are easily formed due to low formation energy introducing severe changes in the bandgap energy of the material as well as additional recombination channels to the photogenerated charge carriers [15], [28], [29].

In addition to tuning the off-stoichiometry of CZTS, the semiconducting properties can be altered by cation and anion alloying.

1.2 Alloying and doping of kesterite

Doping and alloying are two processes used to manipulate mobile charge carriers' concentration in a semiconductor by introducing impurity atoms to the material. In the case of doping, a small amount of impurities (usually less than 1 at.%) is introduced to the host material to tune its electronic properties – donor or acceptor levels are introduced to the band gap. Doping does not result in the formation of a new material phase. Alloying, on the other hand, results in the formation of a solid solution of two or more materials.

Several extrinsic elements have been considered and used for the doping of CZTS without the change in the crystal structure (see Figure 1-3). Mainly alkali elements have been considered - H, Li, Na, and K. In addition, doping with Sb and In has been implemented. The most important findings include kesterite surface passivation with hydrogen, increased charge carrier concentration with Li and K, improved absorber layer morphology with Na, Sb, and K, and reduced interface recombination with In [26], [30]–[33].

Several elements are used for the alloying of CZTS, including Li, Mg, Mn, Fe, Ni, Ag, Cd, In, Ga, Si, Ge, and Sb. Significant improvement in the optoelectronic properties and corresponding solar cell device performance compared to reference devices has been shown only by Ag and Cd single and double cation substitution [34]–[37].

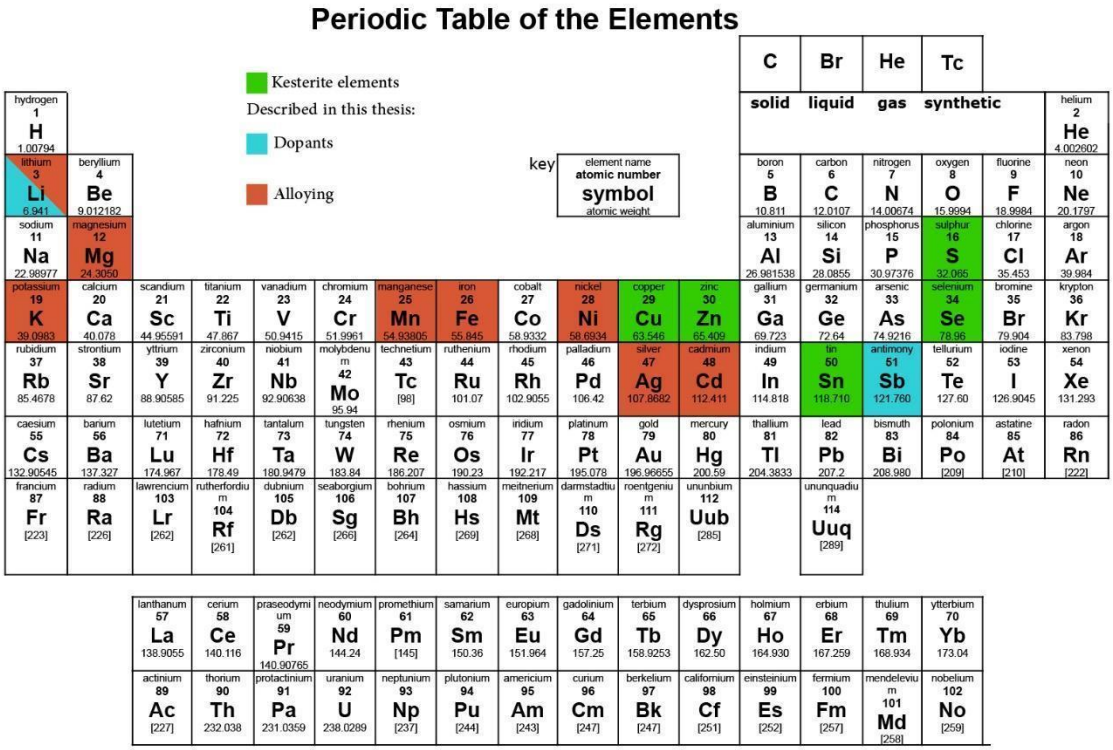

Figure 1-3. Elements used for doping and alloying of CZTS [12].

1.2.1 Doping and alloying of Cu_2ZnSnS_4 with antimony

Aside from Ag and Cd, doping and alloying of CZTS with Sb has attracted researchers attention. Ag and Cd replace Cu and Zn in the kesterite CZTS crystal lattice, respectively; Sb has proven to replace Sn due to the similar ionic radii (Z=51 for Sb and Z=50 for Sn) [38]. Sn introduces deep trap states to CZTS, resulting in strong recombination losses and low Voc values in CZTS solar cells, reaching only about 60% [19]. High recombination rate at the interface of absorber-buffer layers and carrier recombination in bulk were reported as the main sources of this problem. Therefore, suppressing these recombination channels through partial or full replacement of Sn with other elements is of interest for kesterite researchers.

In $CuInSe_2$, the Sb was found to introduce shallow donor defects Sb_{Cu} that suppressed In_{Cu} deep defects and promoted the p to n-type conversion at the CdS/$CuInSe_2$ interface leading to improved solar cell device performance [39]. Since $CuInSe_2$ and Cu_2ZnSnS_4 have both zinc-blend-derived crystal structures, one could expect a similar influence of Sb to the recombination losses in CZTS. However, Zhang et al. has shown that Sb doping

introduces deep defect level 1.1 eV above the valence band maximum, which is not beneficial for the CZTS device performance [40]. They also showed based on the first-principles calculations that starting from a critical concentration (>10^{21} cm^{-3}), Sb creates an isolated half-filled intermediate band at 0.5 eV above the valence band maximum, which enables to increase the photocurrent in the CZTS solar cell device due to sub-band gap absorption. Theoretical defect structure calculations indicate that Sb_{Sn} and Sb_S antisite defects and two Sb_i interstitial defects introduce deep defect energy levels in the band gap of CZTS [38]. Sb_{Sn} antisite defect with ionization energy of 1.1 eV has the lowest formation energy in the system, even lower than Cu_{Zn} acceptor in CZTS. Sb_S antisite defect and the two Sb_i interstitial defects have very high formation energies and are therefore not considered here. On the other hand, Sb_{Cu} and Sb_{Zn} create very shallow donor energy levels in the CZTS band gap, enabling easy ionization of the electrons bound to these defects. High-efficiency CZTS solar cells have been achieved with Zn-rich and Cu-poor composition, which favors Sb_{Sn} antisite and the high population of Sb_{Cu} shallow donors, which could facilitate an n-type conversion at the surface of the p-type CZTS as was reported for $CuInSe_2$ [39].

There are only a few experimental studies reported about the Sb doping of CZTS. Tiwari et al. [30] have studied the Sb doping and Sb and Na co-doping of solution-processed CZTS and found the improved crystallization of the CZTS phase upon doping. Improved crystallization of CZTS upon Sb doping was also reported by Carrete et al. [41]. Sb was found to substitute Sn in CZTS lattice as predicted by theoretical calculations [40]. Moreover, Sb doping and Sb+Na co-doping were found to decrease the Sn-based defect related to room-temperature photoluminescence intensity leading to slightly improved solar cell performance. An increase in the Voc (from 550 mV to 563 mV) and the FF values (from 47% to 58%) with Sb-doped CZTS was detected due to the reduced recombination losses at the CZTS/CdS interface. The temperature-dependent solar cell device measurements were analyzed in a follow-up study by Tiwari et al. [42], where the decrease in the Urbach energy E_U from 56 meV to 48 meV with Sb doping was found to reduce band tails. Temperature-dependent photoluminescence was absent in this study but is of great interest to understand the recombination mechanisms and related defects in Sb doped CZTS.

1.3 Photoluminescence of Cu_2ZnSnS_4

Photoluminescence is a well-known non-destructive, and sensitive tool for studying defects and related recombination mechanisms in semiconductors. PL is the optical radiation emitted by a physical system resulting from excitation to a non-equilibrium state by irradiation with light [43]. For excitation, laser light with energy higher than

the bandgap energy of the material under study has to be used. As a result, an electron is excited to the conduction band, leaving behind a hole in the valence band. When returning to its equilibrium state, the electron and a hole will recombine. There are several recombination mechanisms possible, depending on the defect structure of the material. The most common recombination mechanisms are shown in Figure 1-4, including band-to-band, free-to-bound, donor-acceptor pair, and exciton recombinations.

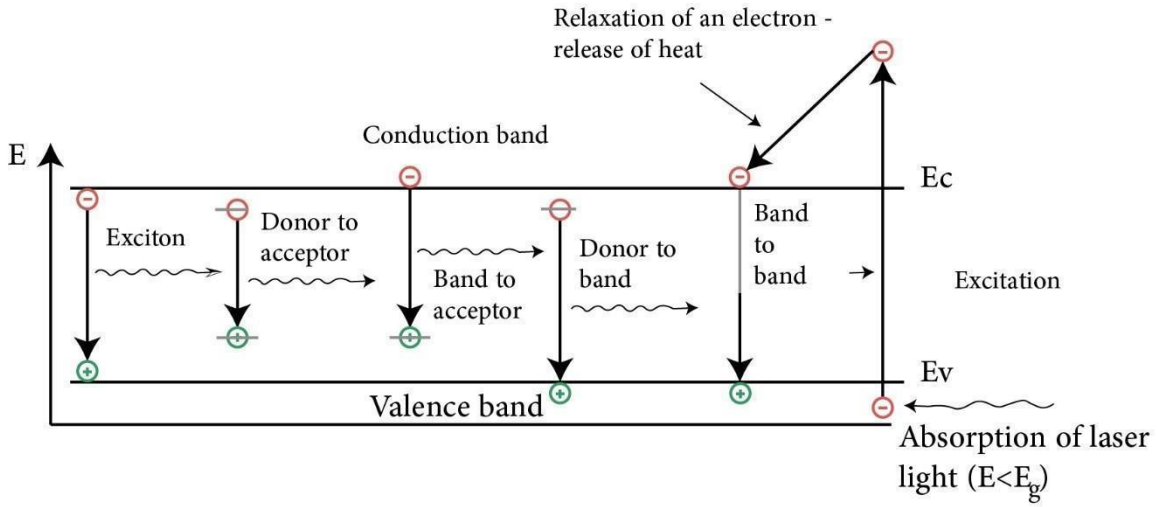

Figure 1-4. Most common bulk recombination mechanisms in semiconductors.

However, in semiconductors with a high concentration of extrinsic or intrinsic defects (>10^{20} cm^{-1}), additional recombination routes are possible. These materials are called heavily doped semiconductors [44], [45]. A large number of non-uniformly distributed charged defects introduce spatial potential fluctuations to the material. This causes widening of the defect levels within the forbidden gap and the formation of valence and conduction band tails (see Figure 1-5). According to the theory [44], the three following recombination channels (see Figure 1-5) usually dominate the PL spectrum of heavily doped semiconductors. The first is a band-to-band (BB) recombination, where a free electron recombines with a free hole. This recombination is normally seen at higher temperatures when the defects are ionized. The second is a band-to-tail (BT) recombination, where a free electron recombines with a hole that is localized in the valence band tail. The third is BI recombination, where a free electron recombines with a hole localized on a deeper acceptor state, which is not overlapping with the valence band tail. The latter means that the acceptor ionization energy has to be larger than the average depth of fluctuations γ.

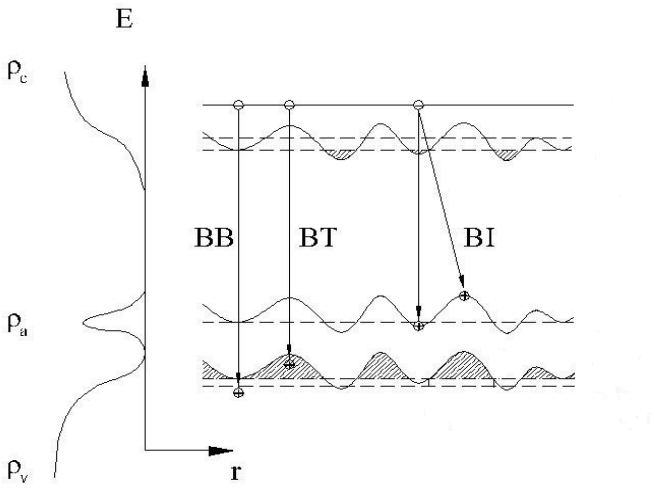

Figure 1-5. Schematic image of the band structure of heavily doped semiconductors together with the main recombination channels: BI, BT, and BB. Because of heavy doping, the band edges fluctuate in space. On the left, the density of state functions ρ_c, ρ_a, and ρ_v of the conduction band, defect state, and valence band, respectively, are presented [46].

Kesterites, which are multinary semiconductors consisting of at least 4 different elements, usually satisfy the conditions of heavy doping [47]–[49]. According to the literature, the low-temperature PL spectrum of CZTS usually consists of single broad (FWHM>100 meV) asymmetric band at ~ 1.3 eV [29], [34], [48], [50]. Although at the same position, the PL band was found to originate from different recombination mechanisms, which is revealed by the temperature and laser power-dependent PL measurements. In the majority of cases, dominant recombination was found to arise from the BI channel involving a free electron and a hole captured by deep acceptor level with ionization energy above 0.01 eV [17], [24], [29]. In addition, the PL emission in CZTS around 1.3 eV was found to result from the donor-acceptor pair recombination [51]. According to the investigations, for the same PL band in CZTS, very different thermal quenching activation energies of 48 meV [52], 39 and 59 meV [47], 20-40 meV [48], and 140 meV [49] have been reported. Also, band to tail and band to band recombinations have been detected in CZTS [46], [50].

The main acceptor defect found in most defect studies, including PL, is the Cu_{Zn} antisite defect that has the lowest formation energy in CZTS [15]. This acceptor defect is considered the dominating hole donating defect in CZTS, and its ionization energy was found to be ~120 meV [49], [53]. In addition to the high concentration of defects, the PL spectra of kesterites are also influenced by the band gap fluctuations due to the Cu-Zn disordering accompanied by the high concentration of defect clusters that can locally decrease the band gap energy of CZTS. For example, (Zn_{Cu}+Cu_{Zn}) defect clusters induce

a local band gap decrease of ~ 0.1 eV [28]. A direct comparison of the X-ray diffraction and PL data in kesterites has shown a correlation between the degree of Cu-Zn disorder and the band gap modification [54]. It was shown that a change in the order parameter from 0 to 0.7 leads to an increase in the band gap up to ~0.2 eV in CZTS [21]. As a result, there are regions in the material where the band gap is largely reduced and the recombination preferably takes place in these regions. A schematic image of the combination of the spatial electrostatic potential and band gap fluctuations is presented in Figure 1-6. One parameter characterizing the band tails is the Urbach energy. Theoretical estimate for tail energy of CZTS (~30 meV) was obtained by Nishiwaki et al. [55]. In experiments, Urbach energy as high as ~ 85 meV has been detected in CZTS and related to the extensive cation disordering [21].

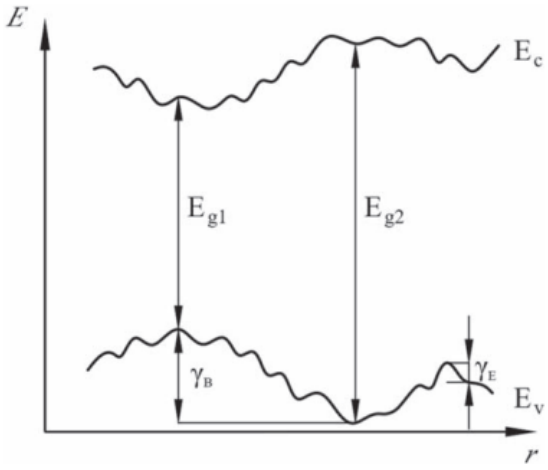

Figure 1-6. Schematic presentation of the band structure of a semiconductor involving electrostatic and band gap fluctuations [6]. Here, γ_E and γ_B are the average depths of the spatial electrostatic potential and band gap fluctuations, respectively.

It is important to emphasize that the defect structure depends not only on the elemental composition but also on the post-growth cooling process or additional thermal treatments that modify the degree of Cu-Zn disordering in kesterites [20]. For example, the influence of the cooling rate of the material after the annealing treatment on the PL emission in CZTS polycrystals was studied by Grossberg et al. [24]. It has been shown that with reduced disordering, there is a change in the dominant radiative recombination process, involving deeper defects in the case of a less disordered material. This can be one reason why reduced Cu-Zn disordering does not significantly improve the device performance.

1.4 Summary and aim of the study

Kesterites as multinary compounds have quite complicated defect structure, which is influenced by the elemental composition, growth and post-growth thermal treatments. Kesterites suffer from strong recombination of lightinduced charge carriers due to bulk and interface recombination. One of major concerns is the detrimental effect of Sn-related deep defects acting as very strong recombination centres. One way to reduce their amount in kesterites is via replacement of Sn with other element such as Sb. Derived from the literature review, the main objective of this master thesis was to study the effect of antimony alloying on the defect structure and related recombination mechanisms in CZTS monograin powders and corresponding monograin layer solar cells. The effect of Sb incorporation on the CZTS monograins is studied by using photoluminescence spectroscopy, Raman spectroscopy, X-ray-diffraction, External Quantum Efficiency (EQE), and temperature-dependent I-V curve (I-V(T)) analysis.

2 Experimental section

2.1 Synthesis of Sb alloyed CZTS monograin powders and preparation of monograin layer solar cells

In this study, the molten salt synthesis-growth method is used for the synthesis of $Cu_2Zn(Sn_{1-x}Sb_x)S_4$ (CZTSbS) monograin powders with different x values 0; 0.01 and 0.05 (hereafter, these values are referred to as 0%; 1%; 5% atomic percentages of Sb for Sn substitution). The powders were prepared by Dr. Kristi Timmo. As precursors, high purity binary compounds Copper Sulfide (CuS; 3N), Tin Sulfide (SnS; 3N), Zinc Sulfide (ZnS; 5N), Antimony Sulfide (Sb_2S_3; 5N), and elemental Sulfur (S; 5N) were used. As for flux material (molten salt media), water-soluble Potassium Iodide (KI; 2N), which has a melting point at 681°C , was used. The precursors were weighed in desired amounts and ratios, mixed in a ball mill, loaded into quartz ampoules, degassed under dynamic vacuum, sealed, and annealed at temperatures above the melting point flux material at 740°C for 136 hours. The processes of formation and growth of semiconductor compound monograin powder crystals take place in the liquid phase of the used flux material. The growth process is finished by cooling the ampoules to room temperature in the air. Crystals of the synthesized powders are released from flux by leaching and rinsing with deionized water. The released monograin powders were dried in a hot-air thermostat at 50 °C and sieved into narrow-sized fractions.

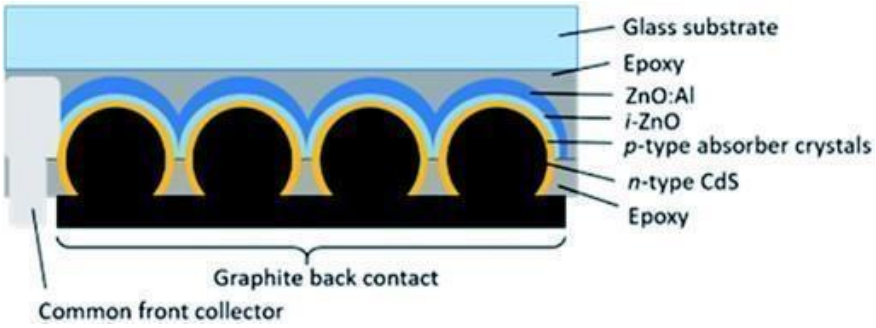

Figure 2-1. Schematic description of the MGL solar cell structure.

$Cu_2Zn(Sn_{1-x}Sb_x)S_4$ monograin powders with varied Sb content were used as absorber materials in MGL solar cells prepared by Dr. Maris Pilvet with the following structure (schematic presentation of the MGL solar cell structure can be viewed in Figure 2-1):

graphite/$Cu_2Zn(Sn,Sb)S_4$/CdS/i-ZnO/ZnO:Al/Ag/glass. In the MGL solar cells, every single CZTSbS crystal covered with the CdS buffer layer works as an individual solar cell

in parallel connection. The photoactive monograin layer was formed by embedding the crystals halfway to a thin epoxy layer. After polymerization of epoxy, the membranes were covered with i-ZnO and conductive ZnO:Al layers using the radio frequency magnetron sputtering system. The silver paste was used to make the front collector onto the ZnO window layer, and the structure was glued onto a glass plate. After removing the supporting plastic foil from the structure, the surfaces of powder crystals were released from the epoxy by etching with concentrated H_2SO_4 for determined times. Finally, the mechanical abrasive treatment was applied to open the back contact area of crystals. A conductive graphite paste dot with an area of 0.052 cm^2 was used for making the back contacts.

Three monograin powders and corresponding MGL solar cell devices were studied in this Master's thesis: pure kesterite Cu_2ZnSnS_4, CZTSbS with 1% Sb and CZTSbS with 5% Sb (input composition).

2.2 Characterization methods

2.2.1 Photoluminescence spectroscopy

PL spectroscopy was used in this thesis as the main experimental tool for studying the defects and related recombination mechanisms in CZTSbS monograins. In this study, two different types of PL measurements were conducted. For the temperature-dependent PL measurements, a Janis CCS-150 single closed-cycle helium cryostat was used. Measurements were made in the temperature range of 20 K-300K. The monograin powders were glued to a copper plate and then with a cryogenic grease mounted on the cryostat's cold finger. LakeShore Model 321 temperature controller was used to control the temperature in the cryostat. The PL system enables to measure a computer-controlled automatic temperature dependence. He-Cd laser (441 nm) was used for PL excitation. An optical chopper modulates the laser beam and distinguishes and amplifies the resulting PL signal reaching the InGaAs photomultiplier tube (PMT) detector. A Horiba Jobin Yvon FHR640 monochromator with 600 lines/mm grating and a Stanford SR810 DSP lock-in amplifier, respectively, were used to resolve and amplify the PL signal. For the laser power-dependent measurements of the PL spectra, neutral density filters were used for altering the power of the incident 441 nm laser beam of the He-Cd laser. The excitation power was varied in the range from 0.77 to 37.1 mW. The laser power-dependent PL measurements were carried out at T = 20K.

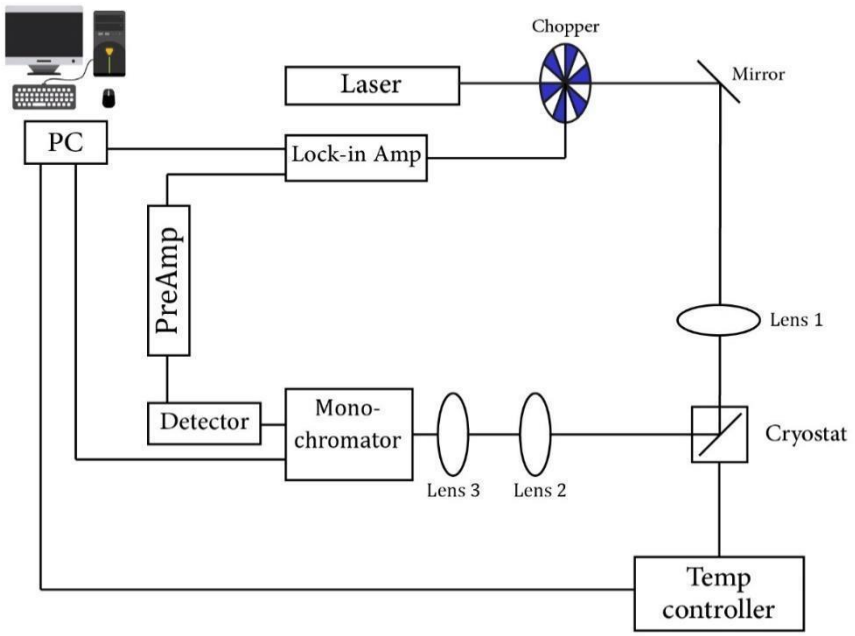

Figure 2-2. The schematic of the photoluminescence spectroscopy measurement system.

2.2.2 Raman spectroscopy

Raman spectroscopy was used in this thesis for identifying the phase composition of the studied materials. Raman spectroscopy is a non-destructive and fast technique, which allows the compositional and crystal structural investigation of the surface region of the materials based on its lattice vibrational spectra. This method is based on the inelastic scattering of light by the material, leading to a change in the frequency of the incident light, also called Raman shift. The room temperature Raman spectroscopy was carried out by Micro-Raman spectrometer Horiba LabRam 800HR. The Nd:YAG laser beam with a wavelength of 532 nm was used for the excitation. The laser spot size on the sample was ~ 10 micrometers in diameter. To analyze the scattered laser light, 1800 lines/mm grating monochromator with a Si CCD detector was used. The Raman measurements were performed in the range 50 – 550 cm^{-1}. For determining the peak positions and half-widths, the measured spectra were fitted by Lorentzian peaks using Fityk software. Afterwards, the resulting peak position values were compared to the literature data to determine the studied samples' phase composition. The full width at the half maximum (FWHM) values of the dominating Raman peaks were used for evaluating the crystalline quality of the samples.

2.2.3 X-ray diffraction

X-ray diffraction method was used in this thesis to determine the crystal structure and phase composition of the studied samples. This method is based on the elastic scattering of a monochromatic X-ray beam by the electrons of the atoms in the crystal. According to the Bragg's law, the XRD pattern of a material consists of peaks arising from the constructive interference of the scattered x-rays. The XRD measurements in this thesis were performed by Dr. Arvo Mere using a Rigaku Ultima IV diffractometer with monochromatic Cu Kα1 radiation (λ = 1.5406 Å) at 40 kV and 40 mA operating with the silicon strip detector D/teX Ultra. The lattice constants were determined by using the Rietveld refinement by Rigaku PDXL version 1.4.0.3 software.

2.2.4 Energy Dispersive X-ray spectroscopy

The elemental composition of the CZTSbS monograin powders was determined by using energy-dispersive X-ray spectroscopy (EDX). EDX utilizes the characteristic X-ray emission excited by an electron beam in the scanning electron microscope (SEM) to quantify the elemental composition of a material. For this thesis, the EDX analysis was performed by Dr. Valdek Mikli using Zeiss Merlin high-resolution scanning electron microscope equipped with the Bruker EDX-XFlash6/30 detector.

2.2.5 I-V curve measurements

Current-voltage (I-V) curve characterization is the simplest and most common tool to evaluate the performance of solar cells. In this thesis, the performance of the CZTSbS based MGL solar cells was characterized by using a Keithley 2400 source meter under standard test conditions (AM 1.5, 100 mW/cm^2) obtained using a Newport class AAA solar simulator. The working area of the MGL solar cells was taken 75% of the total area (total area is the back contact area of the MGL cell: 0.052 cm^2) due to the inactive resin in between the monograins.

It is known that the temperature affects the performance of solar cells. With increasing temperature, the band gap of semiconductors reduces, affecting the essential parameters of solar cells, such as open-circuit voltage (V_{oc}), short circuit current density (J_{sc}), and fill factor (FF). The temperature-dependent I-V measurements indicate the dominating recombination mechanism in the solar cell, whether the recombination dominates it in the bulk of the absorber or at the interface. Therefore, the temperature dependencies of the I-V curves of solar cells were measured in the frame of this thesis

work. For that, the solar cells were mounted on the Janis CCS-150 cryostat's cold finger. I-V measurements were done in the temperature region from 200 K to 300 K with a step of 10 K.

2.2.6 External quantum efficiency

The "external" quantum efficiency (EQE) of a solar cell indicates the amount of current that the cell will produce when irradiated by photons of a specific wavelength. From the shape of the EQE spectra, sources of the photogenerated current losses in the solar cell can be determined. EQE can be used for determining the band gap energy of the absorber material as well as the Urbach energy. EQE also includes the effect of optical losses such as transmission and reflection. EQE measurements were performed in the spectral region of 350-1000 nm using a computer-controlled SPM-2 prism monochromator. The generated photocurrent was detected at 0 V bias voltage at room temperature by using a 250 W halogen lamp.

3 Results and discussion

3.1 Structural and compositional properties of Sb alloyed CZTS monograins

The SEM images of the studied CZTS and CZTSbS monograin powders are shown in Figure 3-1. The fraction size of 63-75 μm was used. Formed crystals have a triangular shape with well-defined planes. According to the EDX analysis, the CZTS and CZTSbS monograin powders had slightly Cu-poor and Zn-rich elemental composition. In CZTSbS with 1% and 5% Sb, the output concentration of Sb could not be detected by EDX. In addition, the presence of ZnS secondary phase was detected in all three samples.

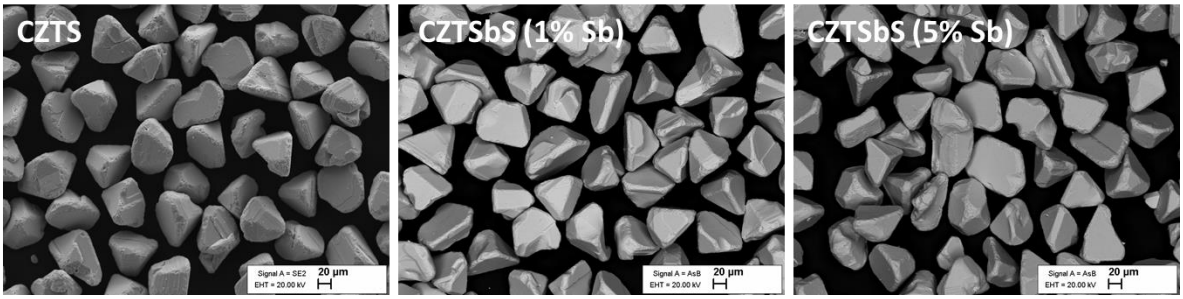

Figure 3-1. SEM images of the CZTS and CZTSbS monograin powders.

Figure 3-2 presents the room temperature Raman spectrum of the studied CZTS and CZTSbS monograin powders together with the fitting result with Lorentzian peaks. The Raman spectra of all three studied samples show the characteristic peaks of kesterite CZTS at 94, 143, 166, 255, 269, 288, 338, 367, and 376 cm^{-1} with minor peak position shifts from sample to sample [17]–[24]. The FWHM value of the main Raman mode at 338 cm^{-1} decreases with increasing Sb content, the corresponding values changing from 3.42 cm^{-1} to 2.70 cm^{-1}. This could be taken as possible evidence of reduced Cu-Zn disordering of the Sb doped samples proposed by Scragg et al. [20]. The peak at 352 cm^{-1} is attributed to the ZnS secondary phase [56], which was also found by EDX.

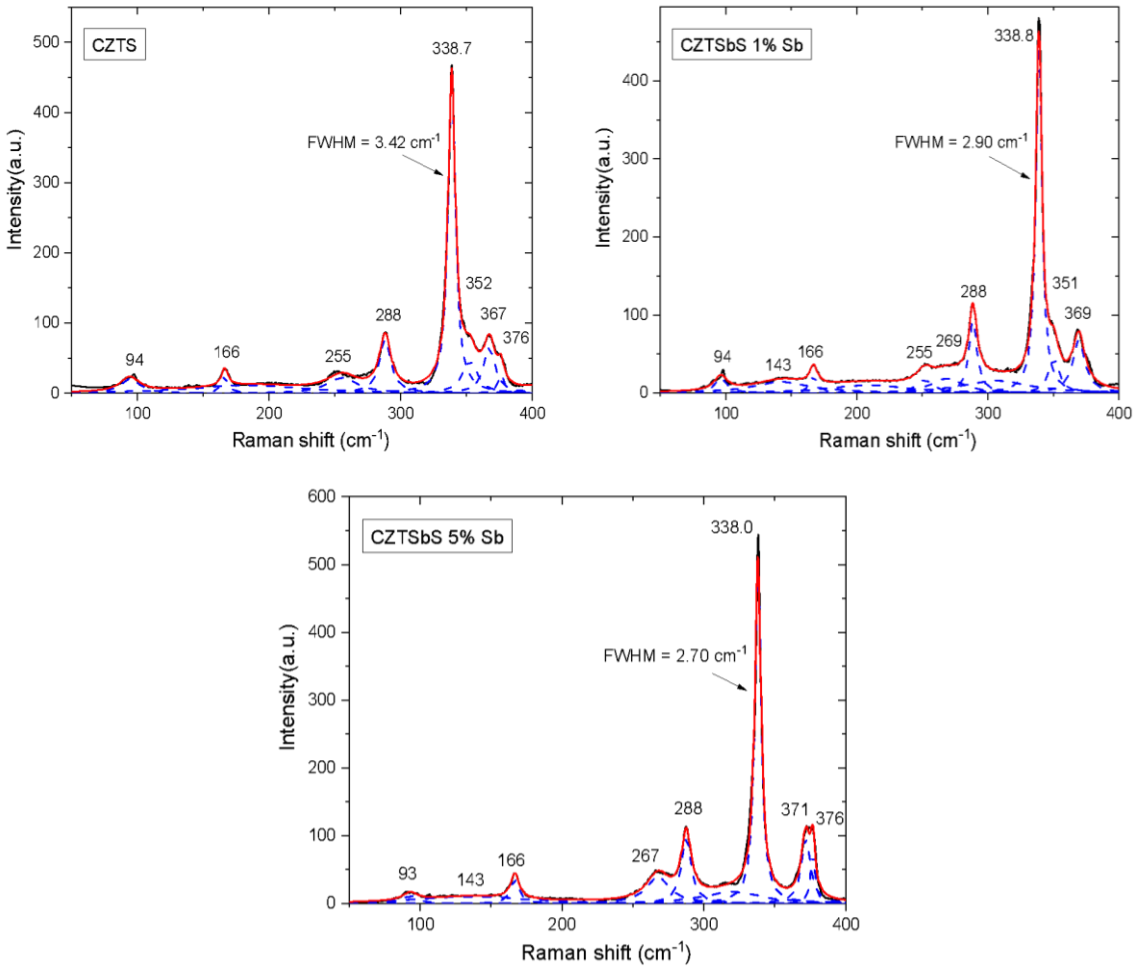

Figure 3-2. Raman spectra of the CZTS and CZTSbS monograin powders together with the fitting result using Lorentzian peaks.

The phase composition was additionally verified by using the XRD method. In addition, the crystal structure and the lattice parameters for the studied samples were determined by this method. The XRD patterns of CZTS and CZTSbS monograin powders are shown in Figure 3-3. It was found similarly to EDX and Raman scattering analysis that the main phase in all three samples is the CZTS with kesterite structure with space group $I\bar{4}$ (ICDD PDF-2 01-084-8521). In addition, the presence of ZnS secondary phase was detected in all three samples, and a minor contribution of famatinite Cu_3SbS_4 phase to the XRD pattern of the Sb containing CZTSbS monograin powders.

Figure 3-4 shows the enlarged view of the (112) peak for the three samples. The diffraction peak shifts slightly towards lower diffraction angles with increasing Sb content, from 28.47 Å to 28.45 Å. This shift in the case of CZTSbS with 5% of Sb indicates the formation of the alloy, which is not observed for the CZTSbS with 1% of Sb. In the latter case, the content of Sb could be at the doping level. Following lattice parameters were determined by the Rietveld refinement procedure: a=b=0.54316 nm

and c=0.10831 nm for CZTS, a=b=0.54314 nm and c=0.10832 nm for CZTSbS with 1% Sb, and a=b=0.54327 nm and c=0.10838 nm for CZTSbS with 5% Sb.

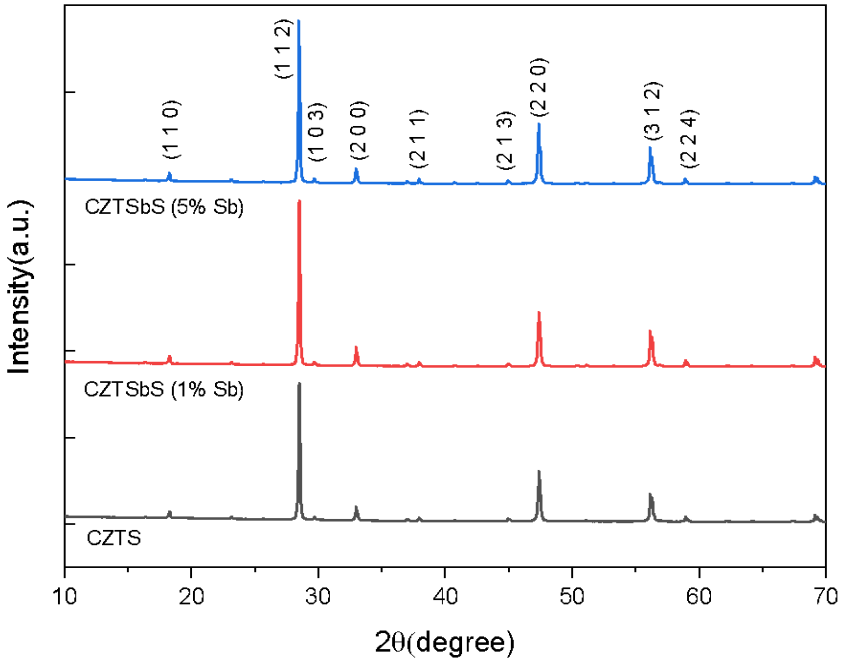

Figure 3-3. XRD patterns of CZTS and CZTSbS monograin powders.

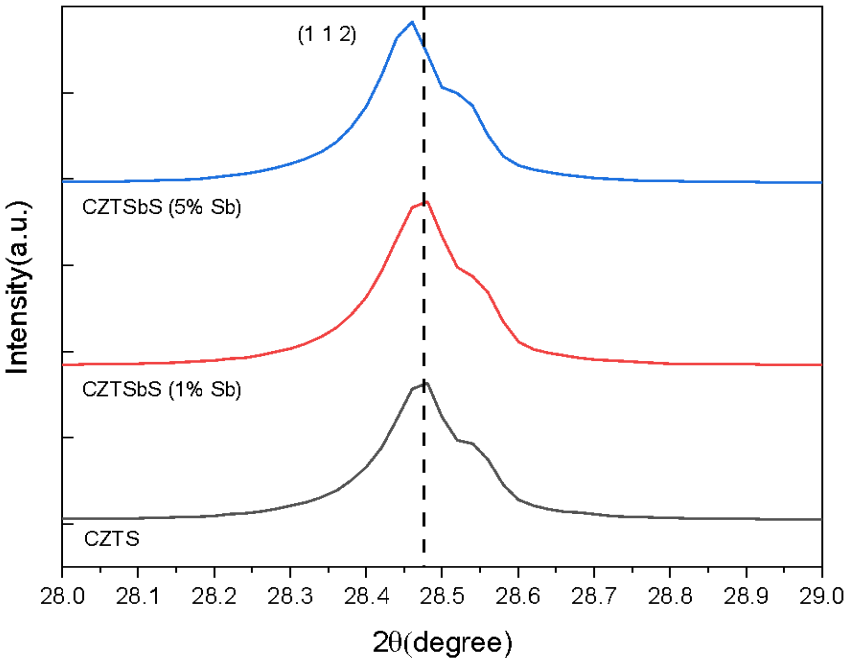

Figure 3-4. Enlarged view of the (112) diffraction peak of CZTS for the three studied samples shifting towards lower diffraction angles with increasing Sb content.

3.2 Photoluminescence of Sb alloyed CZTS monograins

The low-temperature PL spectra (T=20K) of CZTS monograins with different rates of alloying with Sb are presented in Figure 3-5. All spectra are dominated by one broad asymmetric band. It is important to mention that the InGaAs PMT detector sensitivity drops fast, starting from 1.3 eV, which modifies the high-energy side of the PL bands. It can be seen from Figure 3-5 that with increasing the antimony concentration in CZTS, the dominating PL band shifts towards lower energies, the PL band positions being 1.28 eV, 1.25 eV, and 1.23 eV for CZTS, CZTSbS (1% Sb), and CZTSbS (5% Sb), respectively. Moreover, an additional weak deep PL band at around 0.85 eV (PL2) appears in the spectra of CZTSbS (5% Sb) monograins. To reveal the origin of the detected PL bands, temperature and laser power-dependent measurements of the PL spectra were measured and analyzed. All spectra were fitted by using the asymmetric double sigmoid (ADS) function described in [57].

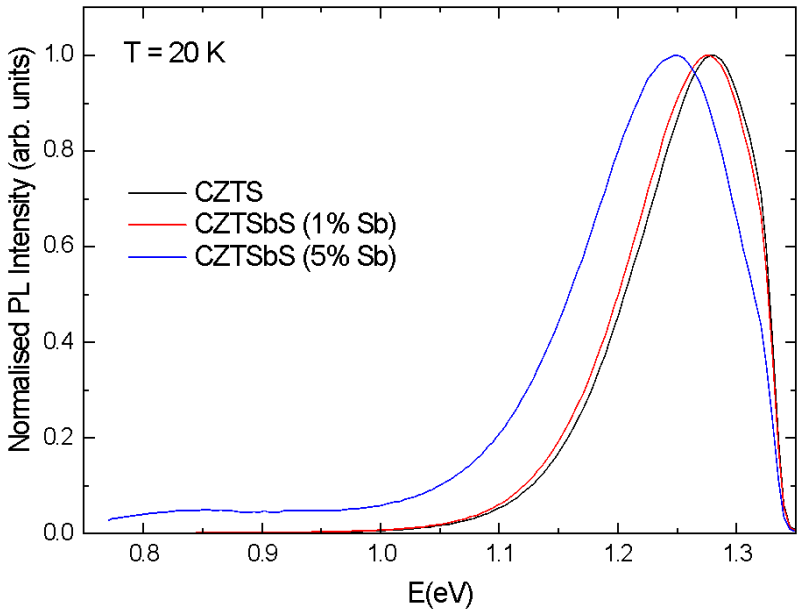

Figure 3-5. Comparison of the low-temperature PL spectra (T = 20K) of the three studied samples with varying Sb content.

The laser power dependencies of the PL spectra of the three studied samples at T = 20 K are presented in Figure 3-6. The laser power was varied in the range from 37.1 mW to 0.77 mW. A strong blue-shift of the dominating PL band position E_{max} with the magnitude of 9 meV/decade, 15 meV/decade, and 15 meV/decade of laser power was

detected for the CZTS, CZTSbS (1% Sb), and CZTSbS (5% Sb), respectively (see Figure 3-7). The asymmetric shape of the PL bands and the strong blue-shift of the peak position with increasing laser power are characteristic of so-called heavily doped semiconductors [44]. In kesterites, the high doping originates from the very high concentration of charged intrinsic defects (>10^{20} cm^{-1}) that cause widening of the defect levels within the forbidden gap and induce the spatial potential fluctuations and formation of valence and conduction band tails (see Figure 1-5). According to the theory, the three following recombination channels usually dominate the PL spectrum of heavily doped semiconductors: BB, BI and BT recombination.

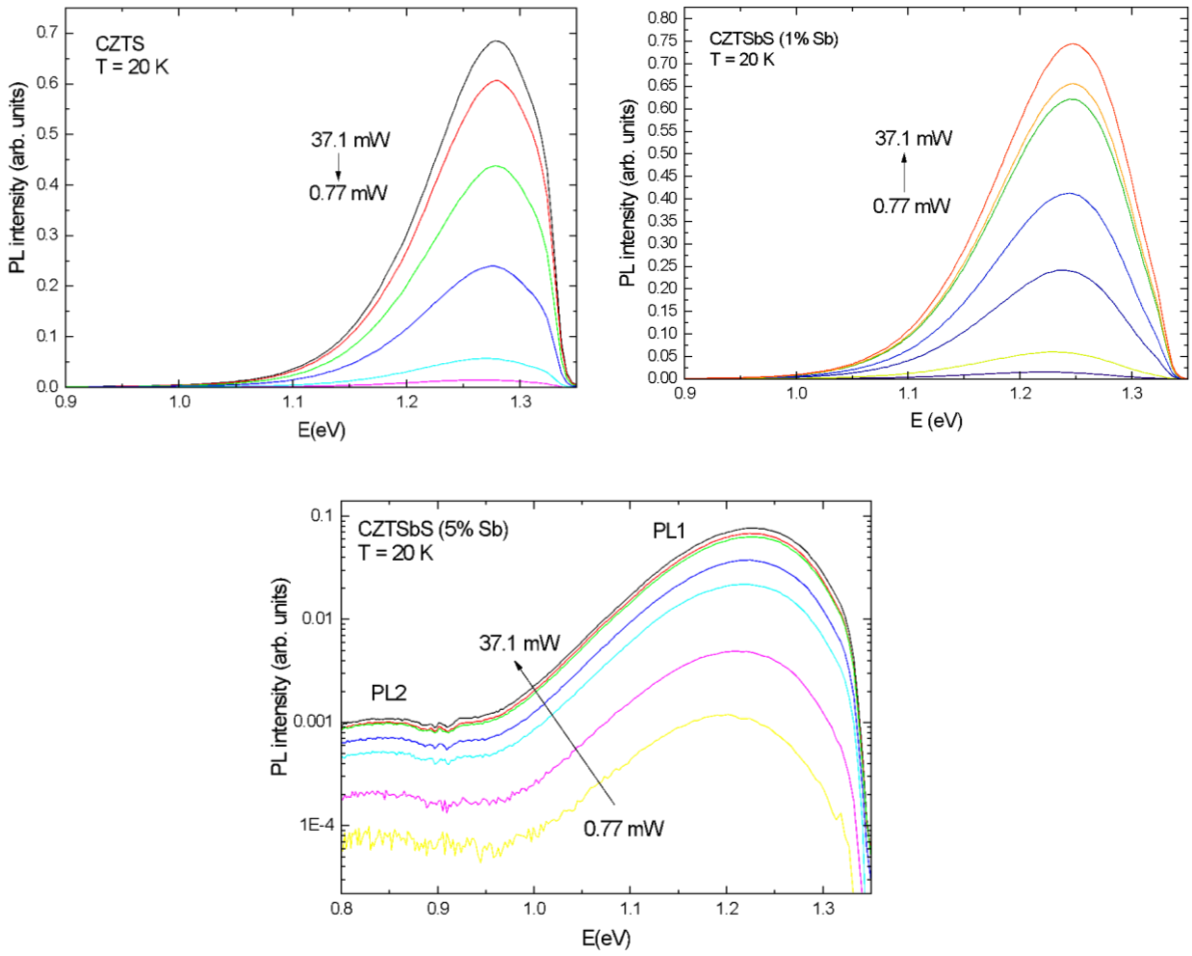

Figure 3-6. Laser power dependence of the PL spectra of the three studied samples with varying Sb content at T = 20K.

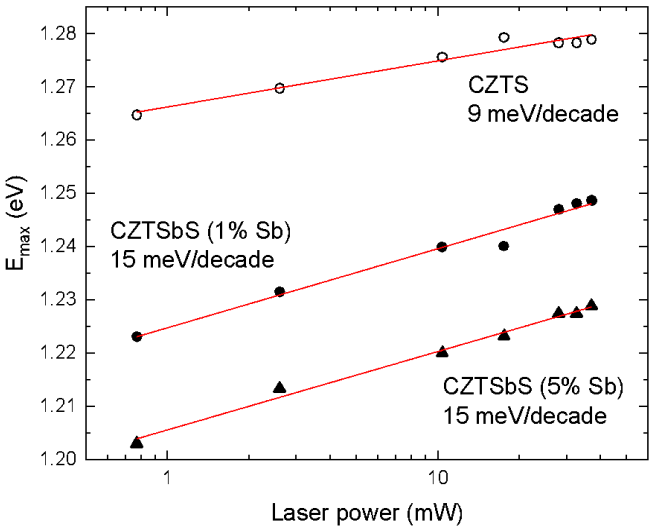

Figure 3-7. Laser power dependence of the dominating PL band positions for the three samples with varying Sb content.

The temperature dependencies of the PL spectra of CZTS and CZTSbS monograin powders are shown in Figures 3-8. A shift of the dominating PL bands towards lower energies with increasing temperature is observed. The temperature dependence of the dominating PL band position E_{max} and the temperature dependence of the bandgap energy [58] is presented in Figure 3-9. It can be seen that at low temperatures, the PL band position follows the temperature dependence of the bandgap energy of CZTS. Starting from approximately 150 K, the PL band starts to shift towards higher energies or stabilizes at its position. This behavior is similar to the CZTS PL bands behavior observed in Ref. [29], where the PL band at 1.35 eV was attributed to the recombination of electrons and holes in the potential well caused by the defect clusters that induce a significant band gap decrease. Shift towards higher energies at higher temperatures could result from the thermal release of carriers from these potential wells.

The thermal activation energies E_T for the dominating PL bands of the three samples were determined from the Arrhenius plot, which shows the linear dependence of the ln $\Phi(T)$ versus 1000/T at high temperatures. This plot describes the theoretical expression for discrete energy level [59]:

$$\Phi(T) = \frac{\Phi_0}{1 + \alpha_1 T^{3/2} + \alpha_2 T^{3/2} exp(\frac{-E_T}{kT})}$$

Where Φ is integrated PL intensity, α_1 and α_2 are the process rate parameters. As can be predicted by the fast quenching of the PL spectra, rather small activation energies were obtained: E_T=56 ± 5 meV for CZTS, E_T=65 ± 4 meV for CZTSbS (1% Sb), and

E_T=25 ± 5 meV for CZTSbS (5% Sb). As was proposed in Ref. [29], these small thermal activation energies are most probably the energies needed for the thermal release of holes from the valence band potential well or electrons from the conduction band potential well. This is proposed as it cannot be related to the ionization of a defect level as the corresponding PL bands should be, in this case, much closer to the band gap of CZTS, which is 1.64 eV at 10 K [58].

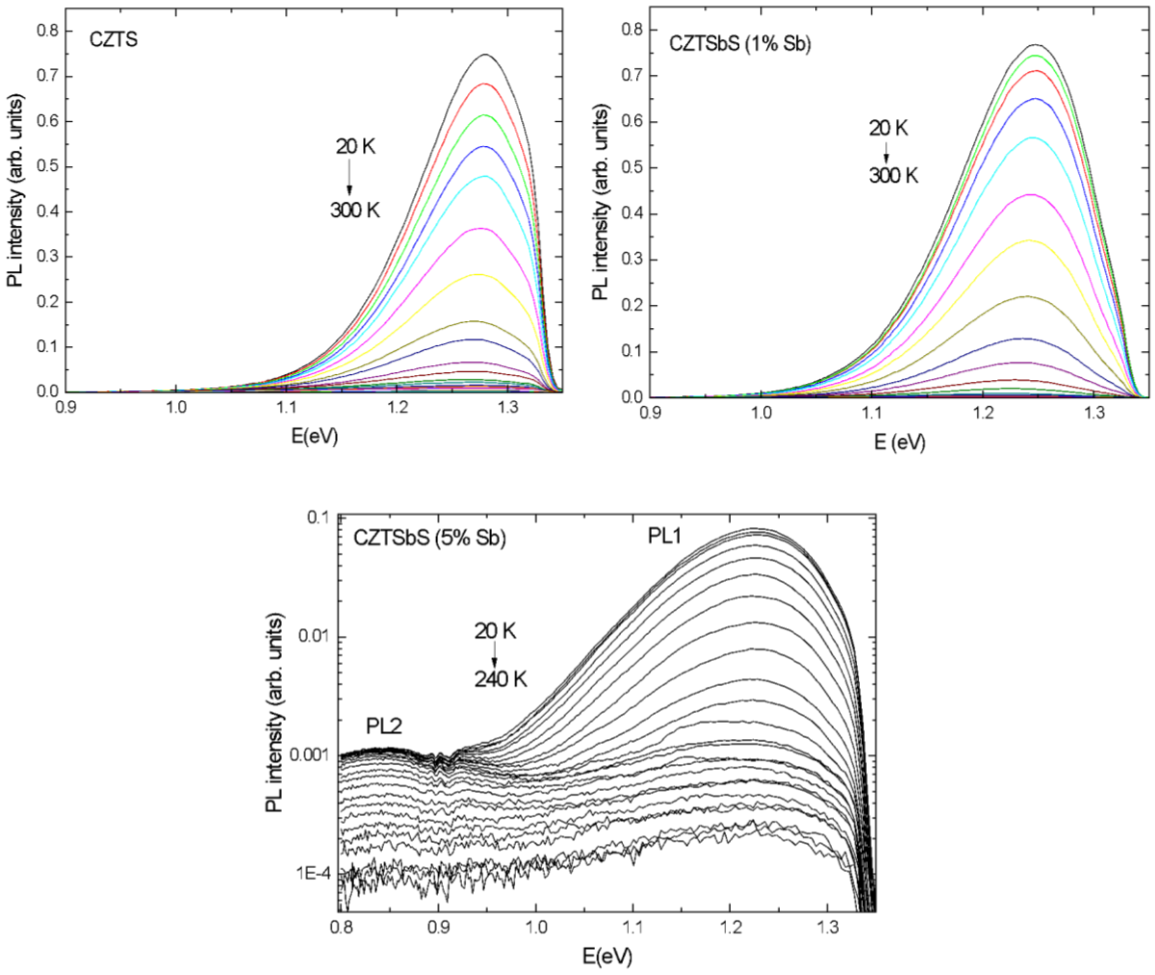

Figure 3-8. Temperature dependencies of the PL spectra of CZTS and CZTSbS monograin powders.

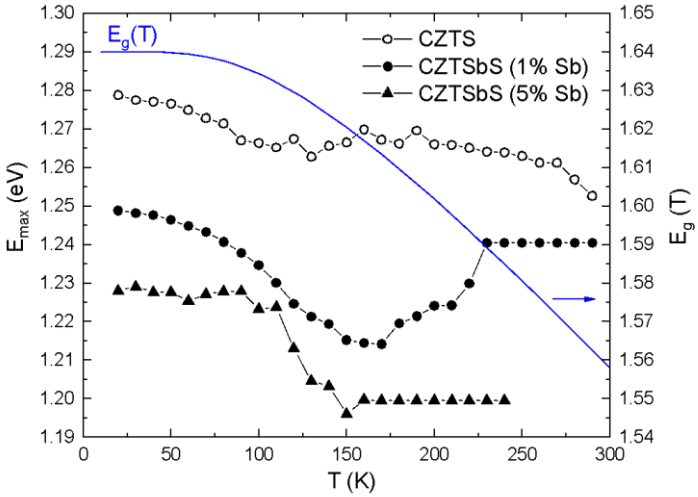

Figure 3-9. The temperature dependence of the dominating PL band position E_{max} together with the temperature dependence of the bandgap energy E_g.

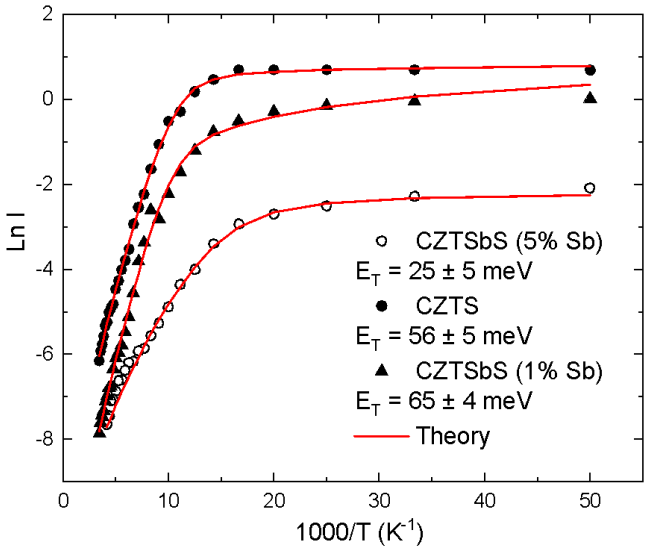

Figure 3-10. Arrhenius plots of CZTS and CZTSbS monograin powders.

Unfortunately, due to the low intensity, the properties of the PL2 band in CZTSbS (5% Sb) could not be studied in detail, and this needs further investigation. We can expect that the relative intensity of this deep PL emission will increase with further increase in the Sb content. In conclusion, the incorporation of Sb into CZTS does not result in the change of the dominating radiative recombination mechanism of CZTS, but additional

deep PL emission at around 0.85 eV is observed in the case of the highest Sb content in this study. In general, deep PL bands are related to deep defects that are detrimental to the photovoltaic device's performance.

3.3 I-V and EQE of Sb alloyed CZTS monograin based solar cells

To determine the effect of Sb incorporation into CZTS monograins on the corresponding solar cell performance, the I-V and EQE measurements on the CZTS and CZTSbS based MGL solar cells were performed. The I-V curves and the EQE spectra for the three solar cells are shown in Figure 3-11 and Figure 3-12, respectively. It can be seen that the overall EQE and the J_{sc} values decrease with the increasing content of Sb in CZTS monograins. The EQE values are rather low, only 15% for the CZTS sample showing the best performance among the studied samples. This could be expected as an additional recombination channel involving deep defects was detected in the PL measurements of the CZTSbS (5% Sb) monograin powders. Moreover, the V_{oc} and the *FF* values show the same trend with increasing Sb content in CZTS. This is opposite trend to the results of the study by Tiwari et al. [30], where Sb was introduced to CZTS in the doping level leading to the improved performance of the corresponding solar cells.

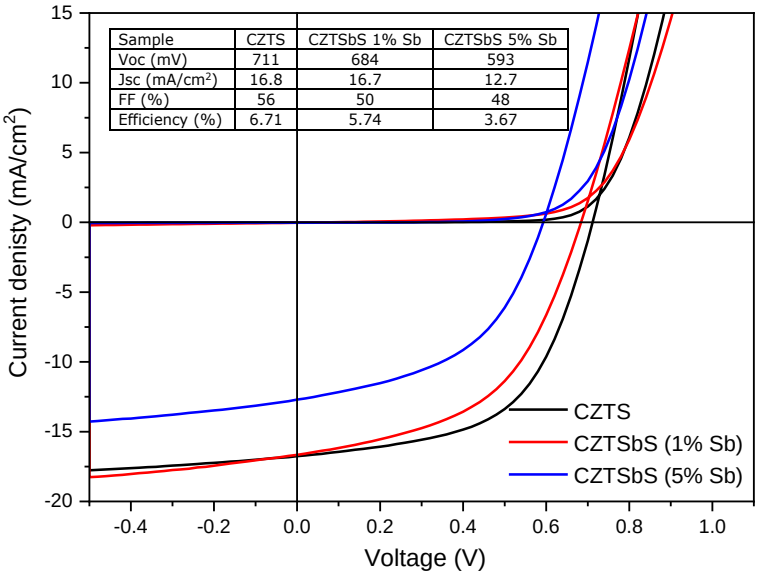

Figure 3-11. The I-V curves of the CZTS and CZTSbS based MGL solar cells.

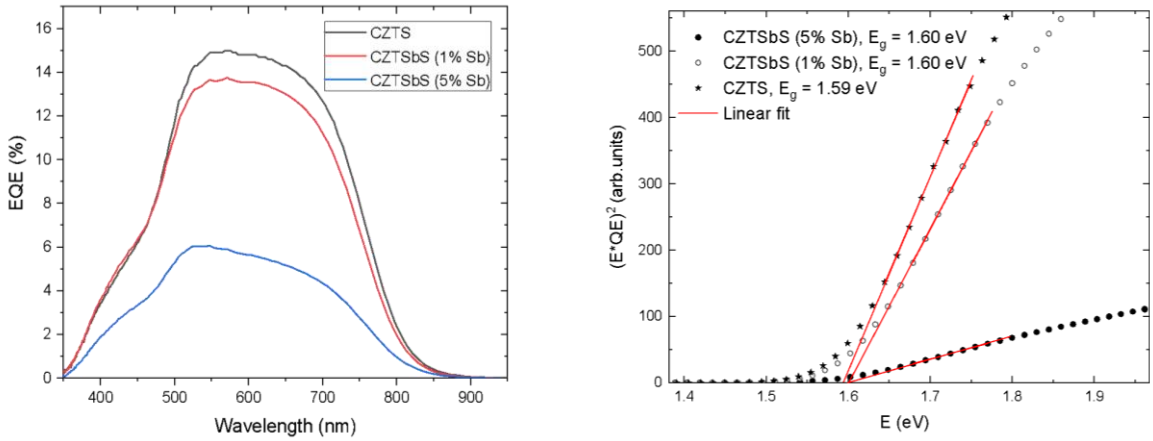

Figure 3-12. (left) The EQE plots of the CZTS and CZTSbS based MGL solar cells and (right) the band gap energies of the absorbers determined from the EQE plots.

I-V characterization was performed under illumination in the temperature range from 200 to 290 K. The behavior of the V_{oc} of the solar cells as a function of the temperature is presented in Figure 3-13. The potential barrier for the dominant recombination mechanism $E_{A,Voc}$ in the solar cell can be calculated by extrapolating the temperature dependence of the V_{oc} to T = 0 K as described by the following equation [60]:

$$V_{oc} = \frac{E_{A.Voc}}{q} - \frac{nkT}{q} ln(\frac{I_{00}}{I_L})$$

where I_L, E_A, Voc, n, k are the photocurrent, the barrier height, the diode ideality factor, and the Boltzmann constant, respectively. The constant q is the electrical charge of the electron, and I_{00} is obtained from the temperature dependence of the dark saturation current I_0. The obtained barrier heights (1104 mV for CZTSbS with 5% Sb, 1158 mV for CZTSbS with 1% Sb and 1126 mV for CZTS) are significantly lower than the band gap energy of CZTS determined from the EQE data (~1.6 eV, see Figure 3-12 (right)). This indicates that the dominating recombination channel in all three solar cells is the interface recombination taking place at the absorber and buffer (CdS) interface.

The defect states in the optical band gap region are represented by Urbach energy (E_u). These localized defects in the band gap region are responsible for the formation of the absorption tail in the absorption spectra, also called the Urbach tail. This value can be extracted from absorption spectra near the absorption onset [30]:

$$\alpha = \alpha_0 exp(\frac{E}{E_u})$$

where a, a_0, E, and E_u are absorption coefficient, absorption constant, incident photon energy, and the Urbach energy. The Urbach energy can be obtained from the slope of the linear part of the plotting ln [-ln(1-EQE)] and E (see Figure 3-13). Urbach energy values of E_U= 23 meV, E_U= 23 meV, and E_U= 24 meV were found for CZTS, CZTSbS (1% Sb) and CZTSbS (5% Sb), respectively. There is minor increase in the Urbach enery with increasing Sb content. Opposite trend was found by Tiwari et al. [30] in the study of Sb doped CZTS thin films.

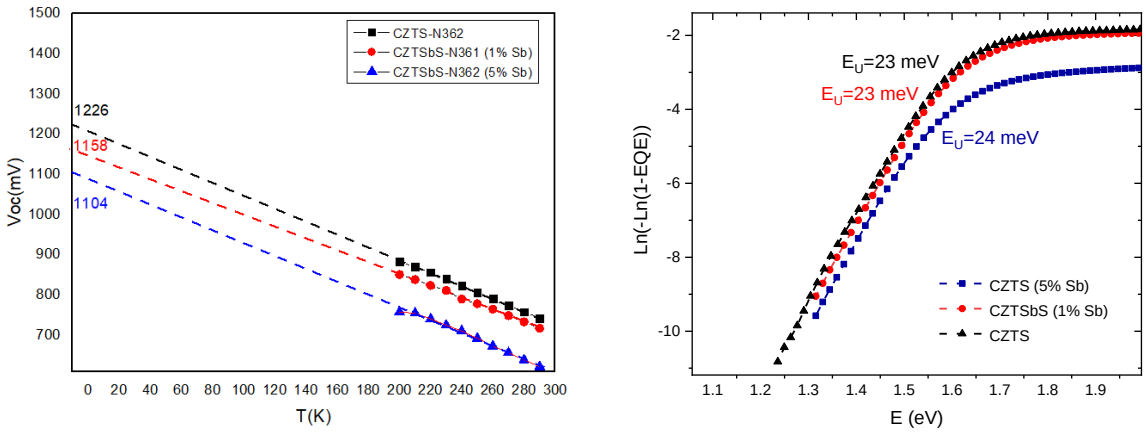

Figure 3-13. a) Temperature dependence of open-circuit voltage, b) estimation of Urbach energy from EQE.

Summary

This master thesis aimed to study the effect of antimony alloying on the defect structure and related recombination mechanisms in CZTS monograin powders and corresponding monograin layer solar cells. Three different monograin powders were studied: pure CZTS, CZTSbS with 1% Sb and CZTSbS with 5% Sb (atomic percentages of Sb for Sn substitution).

EDX analysis confirmed the slightly Cu-poor and Zn-rich elemental composition of the samples, but was unable to detect Sb. The room-temperature Raman spectroscopy was used to study the phase composition and structural quality of the monograins. Narrowing of the main Raman mode of CZTS at around 338 cm^{-1} with increasing Sb content was detected, which could indicate to the reduction of Cu-Zn disordering in the samples. XRD analysis showed the formation of the CZTSbS alloy in the case of the CZTSbS (5% Sb) sample. ZnS secondary phase was detected in all samples by EDX, XRD and Raman analysis. In addition, minor contribution of the famatinite Cu_3SbS_4 secondary phase to the XRD pattern of the Sb containing monograin powders was detected.

Photoluminescence spectroscopy study was conducted as the main part of this research. There is one dominating PL band detected in all samples, which shifts towards lower energies with increasing Sb content, the PL band positions being 1.28 eV, 1.25 eV, and 1.23 eV for CZTS, CZTSbS (1% Sb), and CZTSbS (5% Sb), respectively. An additional weak deep PL band at around 0.85 eV appears in the spectra of CZTSbS (5% Sb) monograins but could not be studied in detail due to low intensity. To reveal the origin of the detected PL bands, temperature and laser power-dependent measurements of the PL spectra were measured and analyzed. It was seen that at low temperatures, the dominating PL band position follows the temperature dependence of the band gap energy of CZTS. Starting from approximately 150 K, the PL band starts to shift towards higher energies or stabilizes at its position. Following thermal activation energies were obtained: E_T=56 ± 5 meV for CZTS, E_T=65 ± 4 meV for CZTSbS (1% Sb), and E_T=25 ± 5 meV for CZTSbS (5% Sb). Considering the small thermal activation energies of the PL bands compared to the distance of the PL band position from the band gap energy of the materials, we propose that the observed PL emission results from the recombination of electrons and holes in the potential well caused by the defect clusters that induce a significant band gap decrease. Shift towards higher energies at higher temperatures could result from the thermal release of carriers from these potential wells. This is also supported by the detected strong blueshift of the dominating PL band with increasing

laser power. In conclusion, according to the PL analysis incorporation of Sb into CZTS does not result in the change of the dominating radiative recombination mechanism of CZTS, but additional deep PL emission at around 0.85 eV is observed in the case of the highest Sb content in this study. In general, deep PL bands are related to deep defects that are detrimental to the photovoltaic device's performance.

As the last part of this research, the effect of Sb incorporation in CZTS on the performance of the corresponding MGL solar cells was studied by EQE and temperature dependent I-V measurements. The results indicated that the EQE, FF, $J_{sc,}$ and V_{oc} parameters were reduced with increasing the content of Sb in CZTS, which results in lower efficiency of the MGL solar cells. From the temperature dependence of the V_{oc}, the interface recombination was identified as the dominating recombination in all studied solar cells. The band gap energies, as well as Urbach energies, were determined for the studied three materials from the EQE plots. The band gaps of E_g = 1.59 eV and E_g = 1.60 eV, and E_g = 1.60 eV for CZTS, CZTSbS (1% Sb) and CZTSbS (5% Sb), respectively, were found. Urbach energy values of E_U= 23 meV, E_U= 23 meV, and E_U= 24 meV were found for CZTS, CZTSbS (1% Sb) and CZTSbS (5% Sb), respectively. There is minor increase in the Urbach energy with increasing Sb content. In conculsion, incorporation of Sb into the CZTS monograin powders under the conditions used in this study did not improve the performance of the CZTS MGL solar cells.

LIST OF REFERENCES

[1] John Bell, Lino Paula, Thomas Dodd, Szilvia Németh, Christina Nanou, Voula Mega, Paula Campos, "EU ambition to build the world's leading bioeconomy—Uncertain times demand innovative and sustainable solutions" *N. Biotechnol.*, vol. 40, pp. 25–30, 2018.

[2] L. Montanarella and P. Panagos, "The relevance of sustainable soil management within the European Green Deal," *Land use policy*, vol. 100, p. 104950, 2021.

[3] H. E. Murdock *et al.*, "Renewables 2020-Global status report," 2020.

[4] Wei Wang, Mark T. Winkler, Oki Gunawan, Tayfun Gokmen, Teodor K. Todorov, Yu Zhu, David B. Mitzi, "Device Characteristics of CZTSSe Thin-Film Solar Cells with 12.6% Efficiency" *Adv. Energy Mater.*, vol. 4, no. 7, p. 1301465, 2014.

[5] T. Ratz, G. Brammertz, R. Caballero, M. León, S. Canulescu, J. Schou, L. Gütay, D. Pareek, T. Taskesen, D-H. Kim, J-K. Kang, C. Malerba, A. Redinger, E. Saucedo, B. Shin, H. Tampo, K Timmo, N. D. Nguyen and B. Vermang, "Physical routes for the synthesis of kesterite," *J. Phys. Energy*, vol. 1, no. 4, p. 42003, 2019.

[6] M. Grossberg, J. Krustok, C. J. Hages, D. M. Bishop, O. Gunawan, R. Scheer, S. Lyam, H. Hempel, S. Levcenco, T. Unold, "The electrical and optical properties of kesterites" *J. Phys. Energy*, vol. 1, no. 4, p. 44002, 2019.

[7] Stéphane Bourdais, Christophe Choné, Bruno Delatouche, Alain Jacob, Gerardo Larramona, Camille Moisan, Alain Lafond, Fabrice Donatini, Germain Rey, Susanne Siebentritt, Aron Walsh, Gilles Dennler, "Is the Cu/Zn disorder the main culprit for the voltage deficit in kesterite solar cells?," *Adv. Energy Mater.*, vol. 6, no. 12, p. 1502276, 2016.

[8] S. Giraldo, Z. Jehl, M. Placidi, V. Izquierdo-Roca, A. Pérez-Rodríguez, and E. Saucedo, "Progress and Perspectives of Thin Film Kesterite Photovoltaic Technology: A Critical Review" *Advanced Materials*. 2019, doi: 10.1002/adma.201806692.

[9] H. Katagiri, N. Sasaguchi, S. Hando, S. Hoshino, J. Ohashi, and T. Yokota, "Preparation and evaluation of Cu_2ZnSnS_4 thin films by sulfurization of evaporated precursors," *Sol. Energy Mater. Sol. Cells*, vol. 49, no. 1, pp. 407–414, 1997.

[10] Dae-Ho Son, Seung-Hyun Kim, Se-Yun Kim, Young-Ill Kim, Jun-Hyung Sim, Si-Nae Park, Dong-Hwan Jeon, Dae-Kue Hwang, Shi-Joon Sung, Jin-Kyu Kang, Kee-Jeong Yang and Dae-Hwan Kim, "Effect of solid-H_2S gas reactions on CZTSSe thin film growth and photovoltaic properties of a 12.62% efficiency device," *J. Mater. Chem. A*, vol. 7, no. 44, pp. 25279–25289, 2019.

[11] W. M. Haynes, *CRC handbook of chemistry and physics*. CRC press, 2014.

[12] Yaroslav E. Romanyuk, Stefan G. Haass, Sergio Giraldo, Marcel Placidi, Devendra Tiwari, David J. Fermin, Xiaojing Hao, Hao Xin, Thomas Schnabel, Marit Kauk-Kuusik, Paul Pistor, Stener Lie and Lydia H. Wong, "Doping and alloying of kesterites," *J. Phys. Energy*, vol. 1, no. 4, p. 44004, 2019.

[13] M.V. Yakushev, M.A. Sulimov, J. Márquez-Prieto, I. Forbes, J. Krustok, P.R. Edwards, V.D. Zhivulko, O.M. Borodavchenko, A.V. Mudryi, and R.W. Martin, "Influence of the copper content on the optical properties of CZTSe thin films," *Sol. Energy Mater. Sol. Cells*, vol. 168, pp. 69–77, 2017.

[14] S. Chen, J.-H. Yang, X.-G. Gong, A. Walsh, and S.-H. Wei, "Intrinsic point defects and complexes in the quaternary kesterite semiconductor Cu_2ZnSnS_4," *Phys. Rev. B*, vol. 81, no. 24, p. 245204, 2010.

[15] S. Chen, A. Walsh, X. Gong, and S. Wei, "Classification of lattice defects in the kesterite Cu_2ZnSnS_4 and $Cu_2ZnSnSe_4$ earth-abundant solar cell absorbers," *Adv. Mater.*, vol. 25, no. 11, pp. 1522–1539, 2013.

[16] S. Das, S. K. Chaudhuri, R. N. Bhattacharya, and K. C. Mandal, "Defect levels in $Cu_2ZnSn(S_xSe_{1-x})_4$ solar cells probed by current-mode deep level transient spectroscopy," *Appl. Phys. Lett.*, vol. 104, no. 19, p. 192106, 2014.

[17] M. Grossberg, J. Krustok, J. Raudoja, and T. Raadik, "The role of structural properties on deep defect states in Cu_2ZnSnS_4 studied by photoluminescence spectroscopy," *Appl. Phys. Lett.*, vol. 101, no. 10, p. 102102, 2012.

[18] S. Schorr, H.-J. Hoebler, and M. Tovar, "A neutron diffraction study of the stannite-kesterite solid solution series," *Eur. J. Mineral.*, vol. 19, no. 1, pp. 65–73, 2007.

[19] S. Chen, X. G. Gong, A. Walsh, and S.-H. Wei, "Crystal and electronic band structure of Cu_2ZnSnX_4 (X= S and Se) photovoltaic absorbers: First-principles insights," *Appl. Phys. Lett.*, vol. 94, no. 4, p. 41903, 2009.

[20] J. J. S. Scragg, L. Choubrac, A. Lafond, T. Ericson, and C. Platzer-Björkman, "A low-temperature order-disorder transition in Cu_2ZnSnS_4 thin films," *Appl. Phys. Lett.*, vol. 104, no. 4, p. 41911, 2014.

[21] M. Valentini, C. Malerba, F. Menchini, D. Tedeschi, A. Polimeni, M. Capizzi, and A. Mittiga, "Effect of the order-disorder transition on the optical properties of Cu_2ZnSnS_4," *Appl. Phys. Lett.*, vol. 108, no. 21, p. 211909, May 2016, doi: 10.1063/1.4952973.

[22] Charlotte Platzer-Björkman, Nicolas Barreau, Marcus Bär, Leo Choubrac, Louis Grenet, Jaeyeong Heo, Tomas Kubart, Alberto Mittiga, Yudania Sanchez, Jonathan Scragg, Soumyadeep Sinha and Matteo Valentini, "Back and front contacts in kesterite solar cells: state-of-the-art and open questions," *J. Phys. Energy*, vol. 1, no. 4, p. 44005, 2019.

[23] Mario Lang, Tobias Renz, Niklas Mathes, Markus Neuwirth, Thomas Schnabel, Heinz Kalt, and Michael Hetterich, "Influence of the Cu content in $Cu_2ZnSn(S,Se)_4$ solar cell absorbers on order-disorder related band gap changes," *Appl. Phys. Lett.*, vol. 109, no. 14, p. 142103, 2016.

[24] M. Grossberg, J. Krustok, T. Raadik, M. Kauk-Kuusik, and J. Raudoja, "Photoluminescence study of disordering in the cation sublattice of Cu_2ZnSnS_4," *Curr. Appl. Phys.*, vol. 14, no. 11, pp. 1424–1427, 2014.

[25] H. Nozaki, T. Fukano, S. Ohta, Y. Seno, H. Katagiri, and K. Jimbo, "Crystal structure determination of solar cell materials: Cu_2ZnSnS_4 thin films using X-ray anomalous dispersion," *J. Alloys Compd.*, vol. 524, pp. 22–25, 2012.

[26] A. Nagaoka, H. Miyake, T. Taniyama, K. Kakimoto, and K. Yoshino, "Correlation between intrinsic defects and electrical properties in the high-quality Cu_2ZnSnS_4 single crystal," *Appl. Phys. Lett.*, vol. 103, no. 11, p. 112107, 2013.

[27] Xianzhong Lin, Ahmed Ennaoui, Sergiu Levcenko, Thomas Dittrich, Jaison Kavalakkatt, Steffen Kretzschmar, Thomas Unold, and Martha Ch. Lux-Steiner, "Defect study of $Cu_2ZnSn(S_xSe_{1-x})_4$ thin film absorbers using photoluminescence and modulated surface photovoltage spectroscopy," *Appl. Phys. Lett.*, vol. 106, no. 1, p. 13903, 2015.

[28] D. Huang and C. Persson, "Band gap change induced by defect complexes in Cu_2ZnSnS_4," *Thin Solid Films*, vol. 535, pp. 265–269, 2013.

[29] M. Grossberg, T. Raadik, J. Raudoja, and J. Krustok, "Photoluminescence study of defect clusters in Cu_2ZnSnS_4 polycrystals," *Curr. Appl. Phys.*, vol. 14, no. 3, pp. 447–450, 2014.

[30] D. Tiwari, M. Cattelan, R. Harniman, A. Sarua, and N. Fox „Impact of Sb and Na Doping on the Surface Electronic Landscape of Cu_2ZnSnS_4 Thin Films" ACS Energy Letters, 3 (12), 2977-2982. 2018.

[31] Zhengfu Tong, Chang Yan, Zhenghua Su, Fangqin Zeng, Jia Yang, Yi Li, Liangxing Jiang, Yanqing Lai, and Fangyang Liu, "Effects of potassium doping on solution processed kesterite Cu_2ZnSnS_4 thin film solar cells," *Appl. Phys. Lett.*, vol. 105, no. 22, p. 223903, 2014.

[32] Feng Jiang, Chigusa Ozaki, Gunawan, Takashi Harada, Zeguo Tang, Takashi Minemoto, Yoshitaro Nose, and Shigeru Ikeda, "Effect of indium doping on surface optoelectrical properties of Cu_2ZnSnS_4 photoabsorber and interfacial/photovoltaic performance of cadmium free In_2S_3/Cu_2ZnSnS_4 heterojunction thin film solar cell," *Chem. Mater.*, vol. 28, no. 10, pp. 3283–3291, 2016.

[33] Jongsung Park, Jialiang Huang, Jaesung Yun, Fangyang Liu, Zi Ouyang, Heng Sun, Chang Yan, Kaiwen Sun, Kyung Kim, Jan Seidel, Shiyou Chen, Martin A. Green, Xiaojing Hao, "The Role of Hydrogen from ALD-Al_2O_3 in Kesterite Cu_2ZnSnS_4 Solar

Cells: Grain Surface Passivation," *Adv. Energy Mater.*, vol. 8, no. 23, p. 1701940, 2018.

[34] Kristi Timmo, Mare Altosaar, Maris Pilvet, Valdek Mikli, Maarja Grossberg, Mati Danilson, Taavi Raadik, Raavo Josepson, Jüri Krustok and Marit Kauk-Kuusik, "The effect of Ag alloying of $Cu_2(Zn,Cd)SnS_4$ on the monograin powder properties and solar cell performance," *J. Mater. Chem. A*, 2019, doi: 10.1039/c9ta07768e.

[35] Shreyash H. Hadke, Sergiu Levcenko, Stener Lie, Charles J. Hages, José A. Márquez, Thomas Unold, Lydia H. Wong, "Synergistic Effects of Double Cation Substitution in Solution-Processed CZTS Solar Cells with over 10% Efficiency," *Adv. Energy Mater.*, vol. 8, no. 32, p. 1802540, 2018.

[36] Chang Yan, Kaiwen Sun, Jialiang Huang, Steve Johnston, Fangyang Liu, Binesh Puthen Veettil, Kaile Sun, Aobo Pu, Fangzhou Zhou, John A. Stride, Martin A. Green, and Xiaojing Hao, "Beyond 11% Efficient Sulfide Kesterite $Cu_2Zn_xCd_{1-x}SnS_4$ Solar Cell: Effects of Cadmium Alloying," *ACS Energy Lett.*, vol. 2, no. 4, pp. 930–936, 2017.

[37] Z. Su, J. M. R. Tan, X. Li, X. Zeng, S. K. Batabyal, and L. H. Wong, "Cation substitution of solution-processed Cu_2ZnSnS_4 thin film solar cell with over 9% efficiency," *Adv. Energy Mater.*, vol. 5, no. 19, p. 1500682, 2015.

[38] X. Zhang, M. Han, Z. Zeng, and Y. Duan, "The role of Sb in solar cell material Cu_2ZnSnS_4," *J. Mater. Chem. A*, vol. 5, no. 14, pp. 6606–6612, 2017.

[39] J.-S. Park, J.-H. Yang, K. Ramanathan, and S.-H. Wei, "Defect properties of Sb- and Bi-doped CuInSe2: the effect of the deep lone-pair s states," *Appl. Phys. Lett.*, vol. 105, no. 24, p. 243901, 2014.

[40] J. Li, X. Zhang, S. Lin, Z. Chen, and Y. Pei, "Realizing the high thermoelectric performance of GeTe by Sb-doping and Se-alloying," *Chem. Mater.*, vol. 29, no. 2, pp. 605–611, 2017.

[41] Alex Carrete, Alexey Shavel, Xavier Fontané, Joana Montserrat, Jiandong Fan, Maria Ibáñez, Edgardo Saucedo, Alejandro Pérez-Rodríguez, and Andreu Cabot, "Antimony-based ligand exchange to promote crystallization in spray-deposited $Cu_2ZnSnSe_4$ solar cells," *J. Am. Chem. Soc.*, vol. 135, no. 43, pp. 15982–15985, 2013.

[42] Devendra Tiwari, Mattia Cattelan, Robert L. Harniman, Andrei Sarua, Neil Fox, Tristan Koehler, Reiner Klenk, and David J. Fermin, "Impact of Sb and Na doping on the surface electronic landscape of Cu_2ZnSnS_4 thin films," *ACS Energy Lett.*, vol. 3, no. 12, pp. 2977–2982, 2018.

[43] H. B. Bebb and E. W. Williams, "Semiconductors and Semimetals," *Acad. Press. New York*, vol. 8, no. 181, p. S8, 1972.

[44] A. P. Levanyuk and V. V Osipov, "Edge luminescence of direct-gap

semiconductors," *Sov. Phys. Uspekhi*, vol. 24, no. 3, p. 187, 1981.

[45] B. I. Shklovskii and A. L. Efros, *Electronic properties of doped semiconductors*, vol. 45. Springer Science & Business Media, 2013.

[46] M. Grossberg, P. Salu, J. Raudoja, and J. Krustok, "Microphotoluminescence study of Cu_2ZnSnS_4 polycrystals," *J. Photonics Energy*, vol. 3, no. 1, p. 30599, 2013.

[47] Y. Miyamoto, K. Tanaka, M. Oonuki, N. Moritake, and H. Uchiki, "Optical properties of Cu_2ZnSnS_4 thin films prepared by sol–gel and sulfurization method," *Jpn. J. Appl. Phys.*, vol. 47, no. 1S, p. 596, 2008.

[48] J. P. Leitao *et al.*, "Photoluminescence and electrical study of fluctuating potentials in Cu_2ZnSnS_4-based thin films," *Phys. Rev. B*, vol. 84, no. 2, p. 24120, 2011.

[49] S. Levcenko, V. E. Tezlevan, E. Arushanov, S. Schorr, and T. Unold, "Free-to-bound recombination in near stoichiometric Cu_2ZnSnS_4 single crystals," *Phys. Rev. B*, vol. 86, no. 4, p. 45206, 2012.

[50] K. Tanaka, T. Shinji, and H. Uchiki, "Photoluminescence from Cu_2ZnSnS_4 thin films with different compositions fabricated by a sputtering-sulfurization method," *Sol. energy Mater. Sol. cells*, vol. 126, pp. 143–148, 2014.

[51] J. Krustok, T. Raadik, M. Grossberg, M. Kauk-Kuusik, V. Trifiletti, and S. Binetti, "Photoluminescence study of deep donor-deep acceptor pairs in Cu_2ZnSnS_4," *Mater. Sci. Semicond. Process.*, vol. 80, pp. 52–55, 2018.

[52] K. Tanaka, Y. Miyamoto, H. Uchiki, K. Nakazawa, and H. Araki, "Donor-acceptor pair recombination luminescence from Cu_2ZnSnS_4 bulk single crystals," *Phys. status solidi*, vol. 203, no. 11, pp. 2891–2896, 2006.

[53] L. Q. Phuong, M. Okano, Y. Yamada, A. Nagaoka, K. Yoshino, and Y. Kanemitsu, "Temperature-dependent photocarrier recombination dynamics in Cu_2ZnSnS_4 single crystals," *Appl. Phys. Lett.*, vol. 104, no. 8, p. 81907, 2014.

[54] D. M. Többens, G. Gurieva, S. Levcenko, T. Unold, and S. Schorr, "Temperature dependency of Cu/Zn ordering in CZTSe kesterites determined by anomalous diffraction," *Phys. status solidi*, vol. 253, no. 10, pp. 1890–1897, 2016.

[55] Mitsutoshi Nishiwaki, Keisuke Nagaya, Masato Kato, Shohei Fujimoto, Hitoshi Tampo, Tetsuhiko Miyadera, Masayuki Chikamatsu, Hajime Shibata, and Hiroyuki Fujiwara, "Tail state formation in solar cell materials: First principles analyses of zincblende, chalcopyrite, kesterite, and hybrid perovskite crystals," *Phys. Rev. Mater.*, vol. 2, no. 8, p. 85404, 2018.

[56] M. Dimitrievska, A. Fairbrother, X. Fontané, T. Jawhari, V. Izquierdo-Roca, E. Saucedo, and A. Pérez-Rodríguez, "Multiwavelength excitation Raman scattering study of polycrystalline kesterite Cu_2ZnSnS_4 thin films" *Appl. Phys. Lett.*, vol. 104, no. 2, p. 21901, 2014.

[57] J. Krustok, H. Collan, M. Yakushev, and K. Hjelt, "The role of spatial potential

fluctuations in the shape of the PL bands of multinary semiconductor compounds," *Phys. Scr.*, vol. 1999, no. T79, p. 179, 1999.

[58] P. K. Sarswat and M. L. Free, "A study of energy band gap versus temperature for Cu_2ZnSnS_4 thin films," *Phys. B Condens. Matter*, vol. 407, no. 1, pp. 108–111, 2012.

[59] J. Krustok, H. Collan, and K. Hjelt, "Does the low-temperature Arrhenius plot of the photoluminescence intensity in CdTe point towards an erroneous activation energy?" *J. Appl. Phys.*, vol. 81, no. 3, pp. 1442–1445, 1997.

[60] U. Rau and H.-W. Schock, "Electronic properties of $Cu(In,Ga)Se_2$ heterojunction solar cells–recent achievements, current understanding, and future challenges" *Appl. Phys. A*, vol. 69, no. 2, pp. 131–147, 1999.